

Ninevah University
College of Electronics Engineering



Brain Tumor Detection by Microwave Imaging Using Deep Learning

Hayder Salah Mahmood

M.Sc. thesis

In

Communication Engineering

Supervised By

Ass. Prof. Dr. Younis M. Abbosh

Ass. Prof. Dr. Diaan M. Ali

2023 A.D.

1445 A.H

Brain Tumor Detection by Microwave Imaging Using Deep Learning

A Thesis Submitted BY

Hayder Salah Mahmood

To

The Council of College of Electronics Engineering

University of Ninevah

In Partial Fulfilment of the Requirements for the Degree of

Master of Science

in

Communication Engineering

Supervised By

Ass. Prof. Dr. Younis M. Abbosh

Ass. Prof. Dr. Daa M. Ali

2023 A.D.

1445 A.H.

بِسْمِ اللَّهِ الرَّحْمَنِ الرَّحِيمِ

رَبِّ قَدْ آتَيْتَنِي مِنَ الْمُلْكِ وَعَلَّمْتَنِي مِنْ تَأْوِيلِ الْأَحَادِيثِ فَاطِرَ
السَّمَاوَاتِ وَالْأَرْضِ أَنْتَ وَلِيِّي فِي الدُّنْيَا وَالْآخِرَةِ تَتَوَقَّئِي مُسْلِمًا
وَأَلْحِقْنِي بِالصَّالِحِينَ

"My Lord! You have indeed bestowed on me of the sovereignty, and taught me the interpretation of dreams; The (only) Creator of the heavens and the earth! You are my Wali (Protector, Helper, Supporter, Guardian, etc.) in this world and in the Hereafter, cause me to die as a Muslim (the one submitting to Your Will), and join me with the righteous."

صَدَقَ اللَّهُ الْعَظِيمُ

سورة يوسف : 101

To

My Mother and My Father

Supervisor's Certification

We certify that the dissertation entitled (**Brain Tumor Detection by Microwave Imaging Using Deep Learning**) was prepared by **Hayder Salah Mahmood** under our supervision at the Department of Communication Engineering, Ninevah University, as a partial requirement for the Master of Science Degree in Communication Engineering.

Signature:

Signature:

Name: Ass. Prof. Dr. Younis M. Abbosh

Name: Ass. Prof. Dr. Daa M. Ali

Department of Communication Engineering

Date: / /2023

Report of Linguistic Reviewer

I certify that the linguistic reviewer of this dissertation was carried out by me and it is accepted linguistically and in expression.

Signature:

Name:

Date: / /2023

Report of the Head of Department

I certify that this dissertation was carried out in the Department of Communication Engineering. I nominate it to be forwarded to discussion.

Signature:

Name: Ass. Prof. Dr: Mahmud A. Mahmud

Date: / /2023

Report of the Head of Postgraduate Studies Committee

According to the recommendations presented by the supervisor of this dissertation and the linguistic reviewer, I nominate this dissertation to be forwarded to discussion.

Signature:

Name:

Date: / /2023

Committee Certification

We the examining committee, certify that we have read this dissertation entitled (**Brain Tumor Detection by Microwave Imaging Using Deep Learning**) and have examined the postgraduate student (**Hayder Salah Mahmood**) in its contents and that in our opinion; it meets the standards of a dissertation for the degree of Master of Science in Communication Engineering.

Signature:

Name:

Head of committee

Date: / /2023

Signature:

Name:

Member

Date: / /2023

Signature:

Name:

Member

Date: / /2023

Signature:

Name:

Member and Supervisor

Date: / /2023

The college council, in its meeting on / /2022, has decided to award the degree of Master of Science in Communication Engineering to the candidate.

Signature:

Name:

Dean of the College

Date: / /2023

Signature:

Name:

Council registrar

Date: / /2023

Acknowledgments

Praise and Thanks to ALLAH Al-Mighty, Lord of the World, who had given me the strength, countless blessings and guidance throughout this journey.

I express my sincere thanks and gratitude to my dearest mother. I was able to do this thesis and reached this position by her efforts, patience and support.

I would like to express my sincere appreciation to my supervisors, Ass. Prof. Dr. Younis M. Abbosh and Ass. Prof. Dr. Daa M. Ali for their invaluable guidance, support, and mentorship throughout my thesis.

Abstract

One of the biggest problems in the medical world is the existence of tumors, especially in the brain. Early detection of the tumor is the key to successful treatment. Current medical imaging techniques, such as computed tomography (CT) scans, magnetic resonance imaging (MRI), and positron emission tomography (PET), have some restrictions. They are bulky in size, expensive, and use ionizing radiation in the case of CT and PET scans, which increases the risk of developing cancer. Microwave imaging is a new hopeful technique that can overcome these restrictions. The microwave system is low-cost, portable, and uses non-ionizing radiation. However, before the system becomes ready for deployment in the hospital, there are still challenges. The reconstructed image has low resolution, is noisy, and blurry due to the use of low frequency and deficiencies in the reconstruction algorithms. This makes detecting and localizing the tumor difficult, especially in its early stages. Furthermore, the decision is subjective and dependent on the physician's experience.

This thesis proposes the use of deep learning to automatically diagnose the existence of the tumor, its size, and its location directly from the raw electromagnetic data collected from a microwave imaging system. A microwave imaging system is designed and simulated in CST software using six antipodal Vivaldi antennas around the head phantom of (HUGO) over the frequency span 1.5 to 4.5 GHz. 628 scans were taken, 308 scans represent cases where tumors exist, with 11 tumor sizes ranging from 0.2 mm to 12 mm radius over 28 different locations in the x-z plane, 4 points in the x-direction, and 7 points in the z-direction. The

remaining 320 scans, represent cases where tumors do not exist. The data was divided into a training set and a test set. A convolutional neural network with 12 filters, each with a 3x3 size, was trained on the training set and then tested with the test set. The results were promising, as the CNN was capable of detecting the existence of the tumor with 100% accuracy on both the training and test sets. It was also able to determine the radius of the tumor with a root mean squared error (RMSE) as small as 0.15 mm and determine the location in the z-direction with an RMSE of 3.15 mm.

Table of Contents

Acknowledgments	VI
Abstract	VII
List of Figures	X
List of Tables	XI
LIST OF ABBREVIATIONS	XII
1 Chapter one: Introduction.....	1
1.1 Background	1
1.2 Literature Review.....	4
1.3 The Problem Statement.....	20
1.4 Thesis Aim	20
1.5 Thesis Layout.....	21
2 Chapter two: Deep learning	22
2.1 Introduction	22
2.2 Artificial Neural Networks [45].....	23
2.3 Deep Learning [45]–[47]	26
2.3.1 Building Blocks of Convolution Neural Network	26
2.3.2 Convolutional Layer	27
2.3.3 Activation Layer	29
2.3.4 Pooling.....	30
2.3.5 Batch Normalization	32
2.3.6 Fully Connected Layer.....	32
3 Chapter three: Application of Deep Learning in Microwave Imaging System	33
3.1 Introduction	33
3.2 Microwave Imaging System	33
3.3 Dataset Construction and Generation	37
3.4 Training Methods.....	41
3.4.1 Training a Convolution Neural Network (CNN) to Detect the Existence of Tumors	41
3.4.2 Training a Convolution Neural Network (CNN) to Predict the Size of the Tumor	43
3.4.3 Training a Convolution Neural Network (CNN) to Predict the Location of the Tumor in the x-z Plane	45
4 Chapter 4: Conclusion and Future Work	50

4.1	Conclusion.....	50
4.2	Future Work.....	52
	References.....	53

List of Figures

Figure 1. 1:	EMTensor 1 st generation brain imaging scanner.....	6
Figure 1. 2:	stroke in a head of a patient (a) MRI scan (b) EMT scan.	7
Figure 1. 3:	(a) ten patch antennas MWS prototype (b) twelve patch antenna MWS	8
Figure 1. 4:	Medfield Diagnostics AB's Strokefinder MD100 device [22]. .	9
Figure 1. 5:	Reconstructed head model image using the DAS-CF imaging algorithm[24].....	11
Figure 1. 6:	MWI system that utilizes antennas of Vivaldi type [27].	12
Figure 1. 7:	Images depicting two different locations of a hemorrhagic stroke [27]	13
Figure 1. 8:	the second system, the phantom has the capability to rotate while the antenna remains fixed [29].....	14
Figure 1. 9:	MWI using a 3-D folded compact antennas [33].....	15
Figure 1. 10:	First prototype of a head-mounted microwave imaging device utilizes thin, flexible antennas placed on a PET-film substrate [35].	16
Figure 1. 11:	The microwave imaging device, designed to be worn as a head strap, incorporates antennas fabricated from textile materials [35].	16
Figure 2. 1:	neural network representation.	24
Figure 2. 2:	typical convolutional neural network.	27
Figure 2. 3:	Convolutional layer.	29
Figure 2. 4:	ReLU activation function.	30
Figure 2. 5:	pooling operation with kernel size 2x2 and stride 2.	31

Figure 3. 1: Microwave Imaging system simulated in CST.	34
Figure 3. 2: antipodal Vivaldi antenna	35
Figure 3. 3: $ S_{11} $ of the designed antenna.	36
Figure 3. 4: far filed radiation pattern of the antenna.....	36
Figure 3. 5: tissues of the voxel head model (HUGO) in CST.....	37
Figure 3. 6: dielectric properties of head tissues. (a) permittivity, (b) conductivity.	37
Figure 3. 7: training/testing loss/accuracy curves of the CNN that detect the existence of tumors.	42
Figure 3. 8: training/testing loss /RMSE of a CNN that predicts the size of the tumor.....	45
Figure 3. 9: training/testing loss /RMSE of a CNN that predicts the z-direction of the tumor.	47
Figure 3. 10 training/testing loss /RMSE of a CNN that predicts the x-direction of the tumor.	47
Figure 3. 11: training/testing loss /RMSE of a CNN that predicts the z-direction of the tumor-non exist dataset.	49

List of Tables

Table 3. 1 tumor-exist scans	38
Table 3. 2 tumor-non exist scans	39
Table 3. 3 Parameters of the training to predict the existence of the tumor.....	42
Table 3. 4 parameters of the training to predict the size of the tumor ..	44
Table 3. 5 parameters of the training to predict the location.....	46
Table 3. 6 parameters of the training to predict the location using tumor-non exist data	48

LIST OF ABBREVIATIONS

Abbreviation	Name
AI	Artificial Intelligence
ANN	Artificial Neural Network
CNN	Convolution Neural Network
CSF	Cerebrospinal Fluid
CT	Computerized Tomography
DAS-CF	Delay-and-Sum Coherence factor
DL	Deep Learning
EM	Electromagnetic
EMT	Electromagnetic Tomography
IFFT	Inverse Fast Fourier Transform
IoT	Internet of Things
ML	Machine Learning
MWI	Microwave Imaging
MWS	Microwave Sensing
MWT	Microwave Tomography
MRI	Magnetic Resonance Imaging
PET	Positron Emission Tomography
R-CNN	Region-based CNN
WHO	World Health Organization
YOLO	You Only Look Once

1 Chapter one: Introduction

1.1 Background

Cancer is a complex and dangerous disease, ranked as the second leading cause of death worldwide. In 2020 alone, it was responsible for an estimated 10 million fatalities, representing one in every six deaths [1]. Tumors, broadly classified as either benign or malignant, result from uncontrolled growth of abnormal cells in any organ of the human body. Benign tumors typically have a uniform cellular structure, grow slowly, and do not spread or invade other tissues. Surgery often provides a cure, and the risk to life is minimal. In contrast, malignant tumors grow quickly, are structurally diverse, and can spread and invade other organs, posing a real threat to life. Even benign tumors in the brain are dangerous because they push against normal brain tissue as they grow, potentially causing severe or life-threatening injuries. Consequently, doctors frequently refer to brain tumors instead of brain cancer [2], [3]. Brain tumor is the 10th leading cause of death worldwide [4]. In the United States, an estimated 700,000 people live with brain tumors, and around 84,000 new cases were diagnosed in 2021, resulting in 18,000 deaths [6]. Worldwide, approximately 300,000 new cases and 250,000 deaths from brain tumors occurred in 2020 [1].

To ensure the best chance of successful treatment, it is crucial to detect tumors as early as possible. Early detection of cancer can significantly increase the chances of the cancer responding to appropriate

therapy, resulting in a higher likelihood of survival, lower morbidity rates, and more cost-effective treatment options. [1], [7].

In the field of medicine, the main imaging techniques for identifying tumors are computed tomography (CT) scans, MRI (magnetic resonance imaging) scanning, and positron emission tomography (PET) [8]. CT scan uses a series of cross-sectional x-ray images to create detailed representations of inside organs and structures. A computer then merges these images into a three-dimensional picture, clearly revealing any tumors or other abnormalities. Using magnets and radio waves, the MRI scanner generates two-dimensional or three-dimensional images of brain tissue. When evaluating the existence of a brain tumor, these pictures are more detailed than those produced by a CT scan. In PET imaging, a tiny quantity of radioactive material (called a "tracer") is put into the circulation of the blood before the test. The tracer will then accumulate in regions where cells are actively dividing. Actively dividing tumor cells will appear as bright spots on the scan. They are popular imaging techniques today; however, they do have some restrictions making them unsuitable for early detection. They are very bulky and expensive, which limits their availability, especially in rural areas, and are hardly affordable for all patients. About three-quarters of the world's population does not have access to safe and inexpensive medical imaging technologies, according to the World Health Organization (WHO). Furthermore, CT and PET scans expose the patients to ionization radiation which increases the risk of developing cancer later in life [2], [6], [8]–[10]. Besides that, manually segmenting, detecting, and extracting the diseased tumor region from medical pictures is a challenging task and time-consuming operation undertaken by radiologists or clinical specialists, and the

accuracy of their work relies only on their expertise in the field [7], [11]. The scientific research community is motivated to develop a new complementary technique to overcome these restrictions.

The portable, low-cost, non-ionization radiation Advantages of microwave systems attracted researchers to employ them to develop a new medical imaging system. Microwave medical imaging relies on the physical principle that the abnormal tissues dielectric properties, such as malignant one, at microwave frequencies are notably different from those of normal tissues. This discrepancy in properties of the dielectric produces a clear contrast in the reconstructed image of the microwave imaging system [12]. An array of antennas constitutes a microwave imaging system, where microwaves are transmitted towards the target objects by the transmitting antenna. These waves are received by the receiving antennas. The reconstructed microwave picture is then created by applying the image reconstruction algorithms to the acquired scattering signals [2], [13]. There are two branches of microwave image reconstruction algorithms, quantitative imaging (microwave tomography) and qualitative imaging (radar-based system). Each method has its benefits and drawbacks. The main differences between these two systems are centered around their frequency characteristics and the way they generate the final image. The MWT system aims to calculate the the human body's dielectric properties, whereas the radar-based method aims to identify the main scatterers within it. multi-band or Narrowband antennas are mainly utilized in the MWT to reconstruct the dielectric properties of the head, whereas the radar-based approach employs a wide-band frequency. MWT gives richer information about the object under screening but its algorithms are complex and computationally

expensive. An image with MWT could take days to be reconstructed. Radar-based images are simple but fast [13] .

1.2 Literature Review

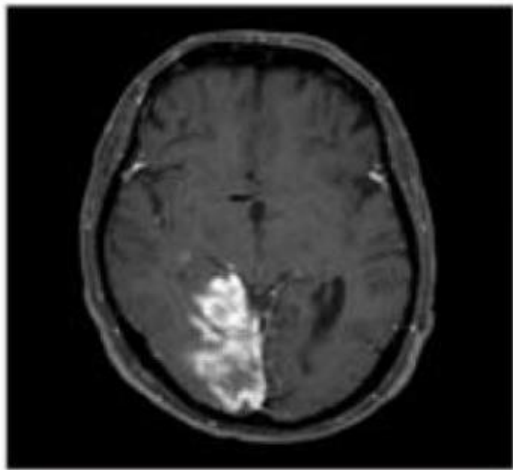
Due to the multiple layers of tissues with high losses, imaging the human head using microwave technologies presents a challenge. However, preliminary studies have indicated that microwave imaging (MWI) of the head is possible and holds potential. Microwave brain imaging traces its roots back to a 1982 paper by Lin and Clark. The paper experimentally verified the cerebral edema (It refers to the buildup of water in the brain) detection using a simple head phantom and a microwave 2.4-GHz signal. Using a head model, it is demonstrated that the microwave signal correlates with variable amounts of excess water. The technology can detect changes in fluid volume by as little as 1 percent [14]. A low-cost triangular patch antenna was designed by H. Trefná and M. Persson. The antenna has the potential to be used as one component within an array designed for monitoring brain strokes. and is intended to be small and lightweight. To enhance impedance matching, For the high-frequency scenario, a bag containing a liquid having a relative permittivity of 78 was positioned between the antenna and the head. In the low-frequency case, the antenna was immersed in the fluid. The researchers proceeded to design and simulate a system comprising eight of these antennas positioned at different intervals. The simulation results, which indicate a return loss difference of up to 3 dB, are quite encouraging and suggest that the proposed system is sensitive enough to detect even minute brain changes [15]. Using computational methods for stroke detection, S. Y. Semenov and D. R. Corfield, presented a

feasibility study regarding the use of MWT to image the human head. Realistic electrical properties were used in the simulator of the head's tissues, and different stroke sizes were utilized. In the configuration, 32x32 and 64x64 transmitter and receiver arrays were utilized. These elements were placed in a circle of 11-centimeter radius around the operating chamber. Both single-frequency and multi-frequency methods were employed across the frequency spectrum spanning from 0.5 GHz to 2 GHz. While a higher frequency of 2 GHz provides better spatial resolution, it was unable to accurately reconstruct the stroke injury region. In comparison to the lower frequencies of 0.5 GHz and 1 GHz when using the single-frequency method. The reason behind this is that as the electromagnetic signal's frequency increases, its attenuation also increases. However, the multi-frequency approach allows the higher frequencies usage of for better capabilities of detection. The critical observation is that low-frequency electromagnetic waves are essential for better signal penetration into the brain. Furthermore, because the skull has a lower water content than other brain tissues like gray matter, white matter, and cerebrospinal fluid (CSF), microwave signals can travel through it with minimal attenuation. Thus, Anticipated results indicate that the skull would not present a significant barriers to penetration of microwave energy into the brain [16]. A new EMT imaging scanner was created by the team based on the numerical analysis conducted earlier. The scanner depicted in Figure 1.1 was utilized during the initial clinical trials to identify strokes in the human brain.

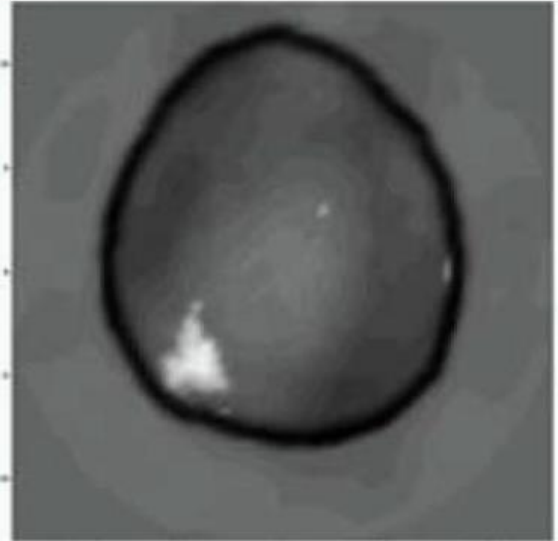


Figure 1. 1: EMTensor 1st generation brain imaging scanner.

Operating with a configuration of 160 ceramic-loaded waveguide antennas, the 3D EMT system functions by utilizing them in a frequency range of 0.9 to 1.1 GHz. A gradient inversion-based iterative solver was employed to reconstruct a head image. The system accurately reconstructed an ischemic stroke image in a patient, and the image resulted closely resembled the MRI image of the same patient. Figure 1.2 demonstrates that the EMT system's capacity for head imaging has been confirmed since the stroke area depicted by the system corresponds well with the MRI image.



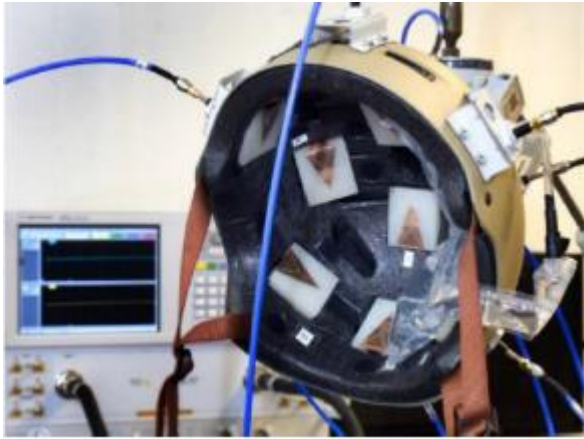
(a)



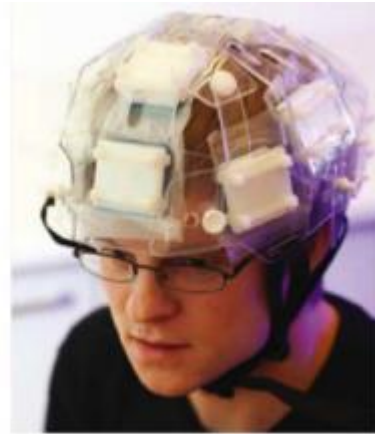
(b)

Figure 1. 2: stroke in a head of a patient (a) MRI scan (b) EMT scan.

Compared to Alternative MWI systems, like wideband radar-based microwave systems, MWT has a significant disadvantage in that reconstructing the head's dielectric map requires more computational resources[17], [18]. A microwave sensing system (MWS) was proposed by A. Fhager and M. Persson with the primary objective of aiding physicians in identifying the type of patient's stroke in order to provide the appropriate treatment. The system utilizes frequencies ranging between 0.3 and 3 GHz, and Figure 1.3 shows two prototypes with twelve and ten antennas positioned surrounding the head.



(a)



(b)

Figure 1. 3: (a) ten patch antennas MWS prototype (b) twelve patch antenna MWS .

Measurements were carried out on patients with known conditions to gather scattered data from different transmission channels. The obtained data was utilized to train the system using a supervised machine learning algorithm that employs a subspace classifier method. According to reports, the system was capable of distinguishing stroke patients from healthy volunteers and identifying the type of stroke present [19], [20].

S. Candefjord created four head phantoms that simulated the dielectric characteristics of blood and gray matter using water, sugar, agar, and salt solutions. Using the system in [19] and all 12 antennas on each phantom, 30 measurements were taken in the frequency range of 0.1-3 GHz, resulting in 120 observations, with two antennas unused. An implemented classification system utilized singular-value decomposition, which achieved 100 percent accuracy by assigning each observation to its corresponding bleeding-class level [19], [21] . In a more recent prototype, J. Ljungqvist, S. Candefjord, M. Persson, and L. Jönsson developed a

system for detecting Head-related conditions like subdural hematoma, as illustrated in Figure 1.4.



Figure 1. 4: Medfield Diagnostics AB's Strokefinder MD100 device [22].

In the clinical trial, the system demonstrated a sensitivity of 100 percent but a specificity of 75 percent. Sensitivity measures the test's accuracy in correctly identifying patients with the disease, while specificity refers to its accuracy in identifying patients with no disease. The prototype is designed to be portable, and it takes approximately 45 seconds to complete a full measurement. However, one significant drawback of these MWS devices proposed is their incapability of determining the size and the location of brain diseases. Such information would be extremely worthy to medical professionals in devising treatment strategies and planning surgeries based on their patients' current conditions [22], [23].

M. Jalilvand and E. Pancera conducted a feasibility study on head imaging using a radar-based technique, employing numerical simulations.

In their simulation, they utilized a Vivaldi antenna due to its high gain and directional radiation beam. The 3D model of head consisted from Different layers of biological tissues, including bone, skin, white matter and grey matter, with a 3-cm-diameter hemorrhagic stroke embedded in it, having similar dielectric properties to blood. They used a bi-static strategy, with one antenna transmitting EM signals and the other receiving the backscattered signal. The antennas frequency of operation ranged from 1.5-5 GHz, and the antennas adjacent distance was maintained at 20 mm. They repeated the process of sending and receiving signals for different predefined positions to scan the head model's entire aperture. They used a modified version of the delay-and-sum (DAS) algorithm, known as DAS Coherence Factor (DAS-CF), to generate the head model's image, as illustrated in Figure 1.5. This study demonstrates a promising application of radar-based stroke detection technology [24]. For the detection of brain cancer, another numerical simulation was conducted by H. Zhang, and B. Flynn. The same technique was applied By employing antennas operating within a higher frequency range, specifically between 5 and 10 GHz. However, it was shown that higher frequencies do not penetrate deeply into the human head, and only tumors located In close proximity to the surface of the head model displayed noticeable Discrepancies observed in the scattered signals. This emphasizes the significance of utilizing low-frequency levels, specifically below 4.5 GHz, to ensure optimal penetration [25].

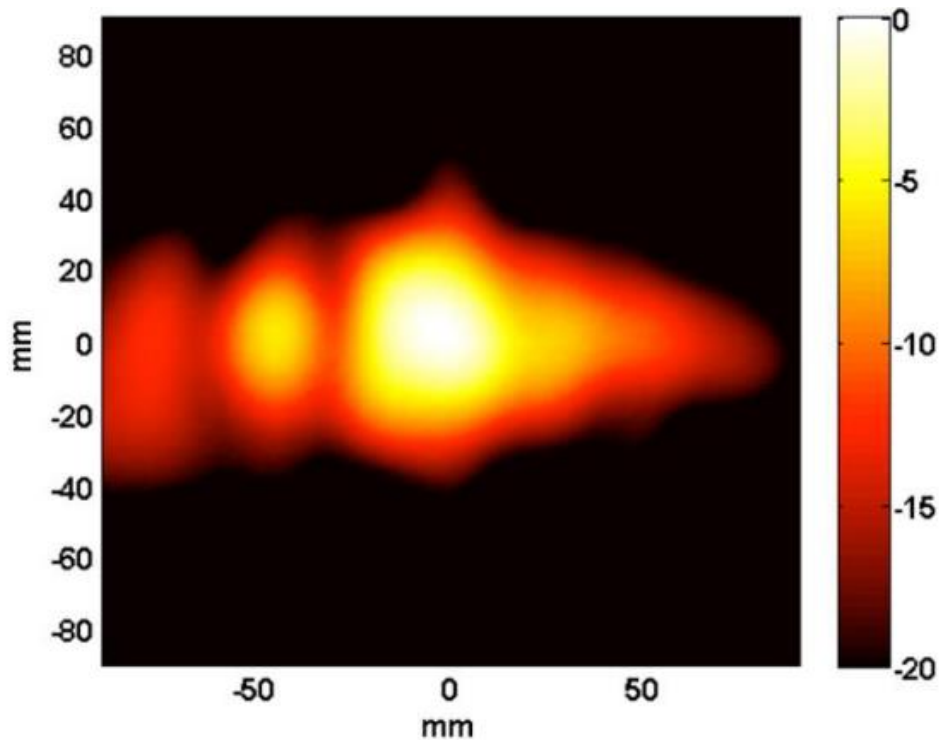


Figure 1. 5: Reconstructed head model image using the DAS-CF imaging algorithm[24]

B. J. Mohammed, A. M. Abbosh, and D. Ireland performed a numerical simulation to detect hemorrhagic stroke by comparing the reflection coefficient (S_{11}) signals acquired from head phantoms representing both healthy and unhealthy conditions. Within the frequency range of 2 to 3.5 GHz, their study revealed that the probing antenna's reflection coefficient experienced a greater loss when exposed to a head phantom with a hemorrhagic stroke in comparison to a healthy head model [26]. Drawing from this observation, they proceeded to develop a comprehensive technique for microwave head imaging based on radar that utilized 16 Vivaldi antennas, as illustrated in Figure 1.6.

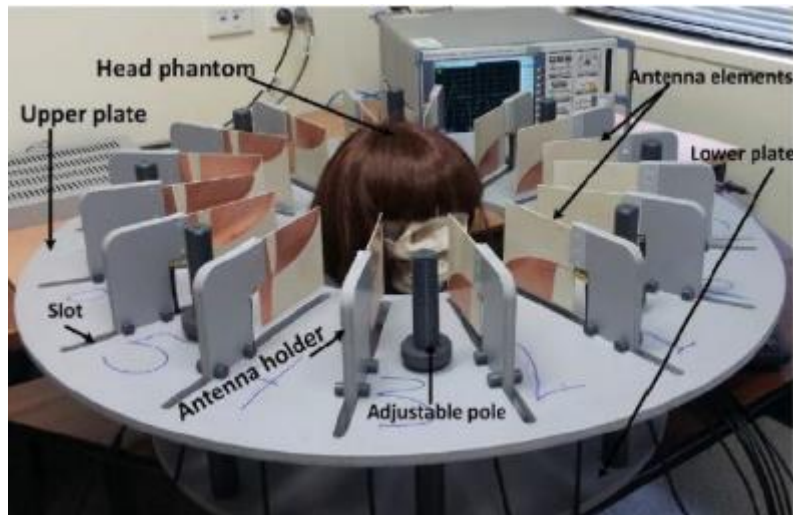


Figure 1. 6: MWI system that utilizes antennas of Vivaldi type [27].

The antennas used in this study function as both transmitter and receiver and operate within a frequency span of 1 to 4 GHz in a monostatic configuration. To avoid mutual coupling and increase the number of signals for image reconstruction, the table on which the head phantom is placed rotates to collect data from different angles. The measured S11 data were converted to time-domain signals using an inverse Fast Fourier transform (IFFT) to apply the confocal imaging algorithm. For testing, a realistic artificial human head phantom was created, consisting from a combination of corn flour ,water, agar, gelatin, sodium azide, and propylene glycol To replicate various brain tissues. A stroke region, simulating blood's dielectric properties, was inserted as an ellipsoid object into the head phantom, and To minimize system complexity, no matching medium was employed. The separation between the antennas and the head model remained constant at 5 mm. The reconstructed images effectively displayed two hemorrhagic stroke objects positioned within the phantoms., as illustrated in Figure 1.7, and the synthesized tissue's

dielectric properties matched the measurements within an error of 3% [27].

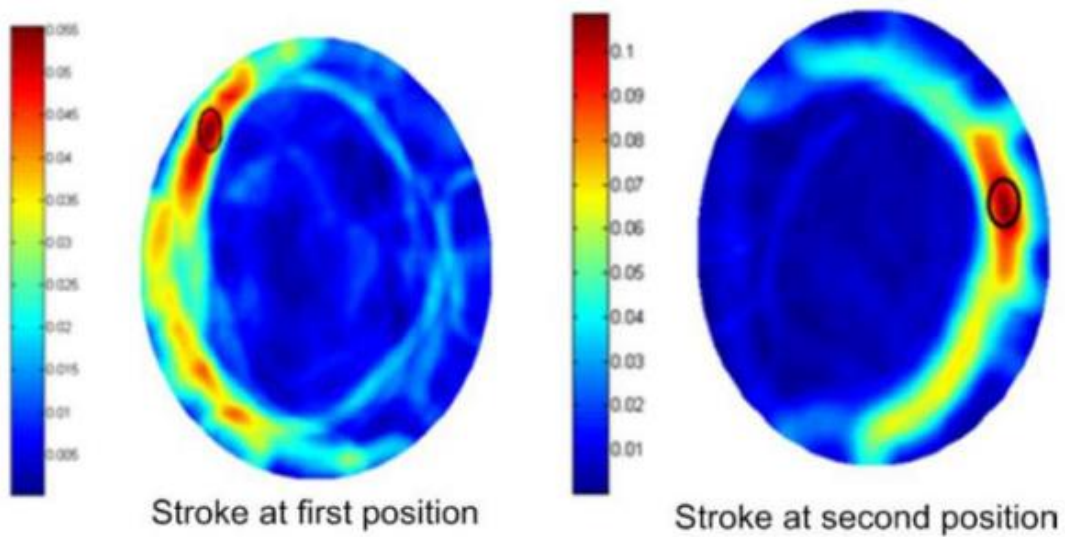


Figure 1. 7: Images depicting two different locations of a hemorrhagic stroke [27]

In order to avoid high losses of energy in the brain at high frequencies, later research replaced the antenna type with small 3-D folded dipole unidirectional antennas Operating within the frequency range spanning from 1.1 to 2.2 GHz. This allows for a balance between penetration depth and image resolution. [28]. The same team of researchers created another system designed to detect traumatic brain injuries using a portable microwave imaging approach. The system, illustrated in Figure 1.8, employs a single unidirectional antenna that covers a frequency range of 1.1 to 3.4 GHz for transmitting and receiving signals to and from a rotatable head phantom. To enable portability of the imaging system, a compact transceiver called the Agilent N7081A was custom-made for signal transmission and data acquisition in the measurement setup The N7081A is a modular WB transceiver device equipped with a bandwidth of 0.1 MHz to 4 GHz, offering a maximum dynamic range of 80 dB. Its operation is managed by an in-house

operating system installed on a personal computer, which can be connected via USB or local-area network for data post-processing [29]. Multiple antenna variations have been reported in [29], [30], and [31]. Using 3-D printing technology, a realistic human head phantom was created to validate the detection capability of the systems[32].

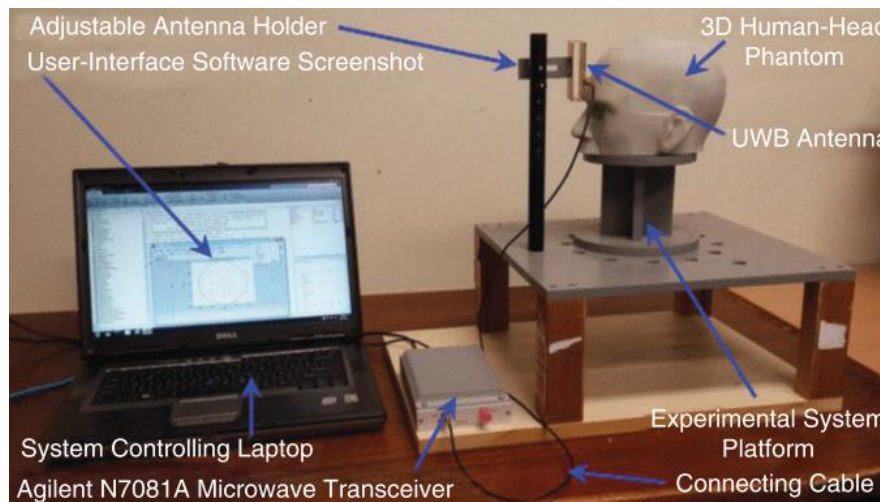


Figure 1. 8: the second system, the phantom has the capability to rotate while the antenna remains fixed [29]

Figure 1.9 shows the improved prototype that included 16 of the 3-D folded compact antennas utilizing a frequency range between 1 and 2.4 GHz that was developed by the same team for future clinical trials [34]. The microwave system designed for portable head imaging aims to provide quick and efficient diagnosis of traumatic brain injuries resulting from various causes such as sports injuries or automobile accidents. The imaging system was tested on two healthy volunteers at three different levels, and the reconstructed images showed no evidence of hematomas [33]. Recent publication [34] describes a new enhancement to the system. Using an advanced combination of a software-defined radio and a solid-state switching network, the system acquires imaging data and functions within the frequency range of 0.52 to 0.85 GHz. With a range of

approximately 106 dB, it can accurately detect realistic brain injuries. Experimental data collection and confocal image generation have confirmed the concept, and images can be generated in under a minute.

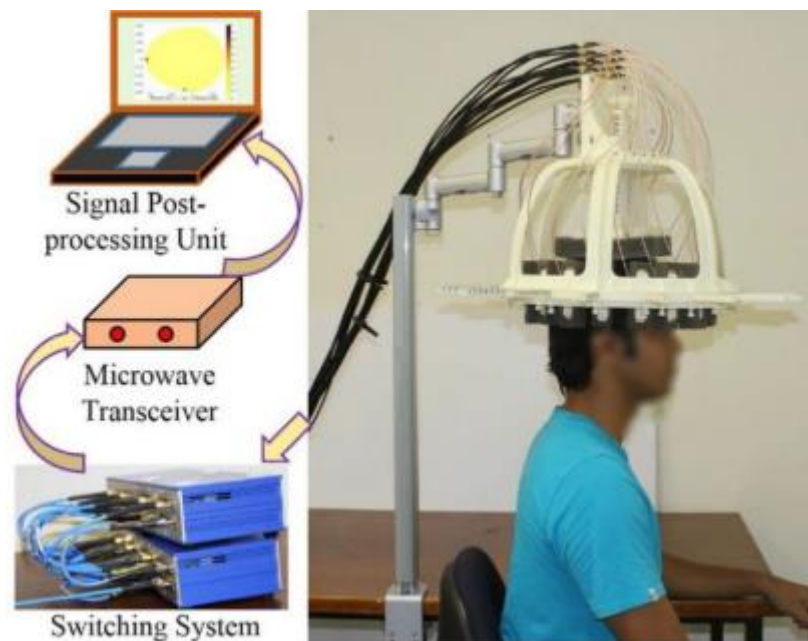


Figure 1. 9: MWI using a 3-D folded compact antennas [33].

There have been numerous studies published that suggest wearable MWI devices can be utilized for head imaging purposes. In one such study, M. S. R. Bashir discusses two different prototypes utilizing low-profile and flexible antennas. The first prototype, illustrated in Figure 1.10, consisted of 12 antennas manufactured on a thin and flexible PET-film substrate. The wearable also contained an absorber material that absorbed any backward signals produced by the antennas. In Figure 1.11, a second prototype was shown, which was a head strap-based wearable MWI device with 12 directional monopole antennas constructed on textile substrates [35]–[37].



Figure 1. 10: First prototype of a head-mounted microwave imaging device utilizes thin, flexible antennas placed on a PET-film substrate [35].



Figure 1. 11: The microwave imaging device, designed to be worn as a head strap, incorporates antennas fabricated from textile materials [35].

The revolution in artificial intelligence (AI) has created new paths for the creation of ground-breaking applications. AI has demonstrated outstanding ability in distinguishing patterns in pictures or data. Thanks to “deep learning”, Today, machines can see, hear, and recognize figures. Deep learning is a special type of algorithm, a subfield of machine learning algorithms which is in its turn a subfield of AI algorithms and has applications in several fields, including autonomous vehicles, health, computer vision, and the Internet of Things (IoT). Researchers are now fascinated by the biomedical applications of machine learning and

artificial intelligence, particularly in the field of anomaly detection to enable automated tumor diagnosis [11].

W. Shao and Y. Du, investigated the reconstruction of microwave images using a method of deep learning. The neural network can convert measured microwave signals acquired from a 24x24 antenna array operating at 4 GHz into an image of 128x128 pixels. To reduce the difficulty of training, an autoencoder that represented high-resolution images (128x128) as 256x1 vectors was created; then a second neural network that mapped microwave signals to the compressed features (256x1 vector) was created. When both neural networks are successfully developed, they can be combined to form a complete network for reconstruction. The current two-stage training method makes training deep learning networks (DLNs) for inverse reconstruction less challenging. The developed neural network is validated by simulation examples and experimental data involving objects of varying shapes/sizes, locations, and dielectric constants between 2 and 6 [38]. A. Yago, M. Cavagnaro, and L. Crocco used A convolutional neural network (CNN)-based U-Net segmentation framework to mask the tumor object in MW imaging. The main goal is to create a reliable framework that can retrieve unknown target shapes without relying on user input. To achieve this, the suggested approach uses the orthogonality sampling method, an inversion technique that can quickly provide a visual estimation of target shapes. The output of the qualitative inversion is then processed by U-Net, a fully convolutional deep learning network. U-Net generates binary masks that can separate the scattering objects (foreground) from the background, thus representing the geometrical properties of the targets. The framework was evaluated using only simulated data and no experimental

framework was implemented [39]. N. M. Dipu, S. A. Shohan, and K. M. A. Salam proposed two deep learning-based techniques for brain tumor identification and classification using the cutting-edge object detection framework YOLO (You Only Look Once) and the deep learning library FastAi. This research was conducted on a subset of the BRATS 2018 dataset, which included 1,992 Brain MRI images. The accuracy of the YOLOv5 model was 85.95 percent, whereas the accuracy of the FastAi classification model was 95.78 percent [40]. E. Avşar and K. Salçin, analyzed MRI scans to identify tumor-containing regions and categorize these regions into three tumor types: meningioma, glioma, and pituitary. In this study, faster Region-based Convolutional Neural Networks (faster R-CNN), a deep learning technique, have been built using the TensorFlow library. A publicly available dataset of 3,064 MRI brain scans of 233 patients (708 meningiomas, 1,426 gliomas, and 930 pituitaries) was used to train and evaluate the classifier. It has been demonstrated that the faster R-CNN approach can achieve 91.66 % accuracy. Due to the small training dataset, the model's outperformance was rather low, and it failed to classify the small tumor in the photos [41]. H. Dong, G. Yang, F. Liu, Y. Mo, and Y. Guo used a method for the fully automatic segmentation of brain tumors using U-Net-based deep convolutional networks. Multimodal Brain Tumor Image Segmentation (BRATS 2015) datasets containing 220 high-grade brain tumors and 54 low-grade tumor cases were used to evaluate the method. This method is capable of identifying tumors, and cross-validation has demonstrated the method's ability to obtain promising segmentation results efficiently [42]. In their research, A. Hossain presented a method for detecting brain tumors using a portable electromagnetic imaging system and a YOLOv3 deep neural

network model. To gather scattering parameters, they utilized a nine-antenna array setup with a tissue-mimicking head phantom, where one antenna acted as a transmitter and the other eight as receivers. The resulting images were reconstructed using a modified delay-multiply-and-sum algorithm. By collecting fifty images from different head regions, they generated a final dataset of 1000 images, including fifty samples with single and double tumors, which were augmented for training, validation, and testing. Eighty percent of the dataset was used for training, ten percent for validation, and the remaining ten percent for testing. The accuracy and F1 score achieved were 95.62% and 94.50%, respectively, and the training accuracy and validation losses were 96.74% and 9.20%, respectively. The performance of detection was evaluated using various image datasets [9]. A study conducted by A. Hossain, M. T. Islam, and A. F. Almutairi focused on using the YOLOv5 object detection model based on deep learning to automatically classify and detect brain abnormalities in a portable microwave head imaging system (MWHI). The MWHI system collected 400 RMW image samples at the outset, consisting of both non-tumor and tumor(s) in different locations, with each RMW image sized 640 by 640 pixels. The images were pre-processed and augmented to create a training dataset of 4,400 images. The models were trained using 80 percent of the images and tested with the remaining 20 percent, while 20 percent of the training dataset was used to validate the models. The performance of detection and classification was assessed using three variants of the YOLOv5 model, namely, YOLOv5s, YOLOv5m, and YOLOv5l. The study determined that the YOLOv5l model outperformed YOLOv5s and YOLOv5m, achieving an accuracy, precision, sensitivity, specificity, F1-score, mean average precision (mAP), and classification loss of 96.32

percent, 95.17%, 94.98%, 95.28%, 95.53%, 96.12 percent, and 0.0130 percent, respectively. The YOLOv5l model correctly detected tumors in RMW images by predicting a bounding box and abjectness score and classifying them as benign or malignant [2].

1.3 The Problem Statement

The reconstructed images from microwave imaging systems have a low spatial resolution, noisy and blurry due to the use of low frequency, and the lack of robust reconstruction algorithms. This confuses the physician to detect and localize the tumor, especially in its early stage, and in the end, the decision is subjective to the physician's experience. Most of the machine learning research has focused on identifying the existence of tumors in medical images. No research has been done to determine the size of the tumors. No large-scale research has been done to determine the location.

1.4 Thesis Aim

To address the aforementioned challenges in microwave imaging systems, this thesis proposes the use of deep learning to automatically diagnose the existence of tumors, size, and location directly from the raw data collected from a microwave imaging system. CST software will be used to design and simulate the transmitted signals in microwave frequencies and received signals. The received signals by many antennas are to be processed using a suitable deep-learning neural network

1.5 Thesis Layout

The thesis is organized as follows:

Chapter one gives an introduction and literature review.

Chapter two presents an overview of deep learning and neural networks.

Chapter three explains the design of the MWI system in CST and the data generation, presents the results and gives a discussion of the results.

Chapter four gives the conclusions and suggestions for future work.

2 Chapter two: Deep learning

2.1 Introduction

In order to address a computational issue, an algorithm is essential. A series of steps need to be carried out to convert input into output. For instance, a sorting algorithm can be devised, where a list of numbers is the input, and an arranged list of those numbers is the output. Sometimes there is no algorithm for some tasks or it is very difficult to make one, such as distinguishing spam emails from non-spam. The nature of the input is known, which is a character-based email document. The expected output is known as either: a yes/no output indicating whether or not the message is spam. It's unknown how to convert the input into the output. What can be considered spam, varies over time and between individuals. Instead of creating an algorithm by hand, let the computer(machine) "learn" this input-output relationship automatically from a given input-output pair of data. That is machine learning. And the algorithms that give the machines this ability are called machine learning algorithms [43]. In general, any problem in machine learning can be categorized into one of two broad categories: supervised learning and unsupervised learning. In supervised learning, a data set is provided and the correct output is given with the assumption that there is a correlation between the input and output. Regression and classification problems are categories of supervised learning problems. In a regression problem, results within a continuous output are to be predicted by mapping input variables to a continuous function. In a classification problem, discrete output results are to be predicted. In other words, it's an attempt of mapping input variables to discrete classes. Unsupervised learning, on the other hand, enables one to approach problems with limited or no knowledge of what the expected

outcomes should be. a structure can be derived from data even if the output is unknown. This structure can be derived by clustering the data based on the relationships between the variables. Some machine learning algorithms are artificial neural networks, support vector machines, k-nearest neighbors, and more. Deep Learning refers to the process of training Neural Networks, sometimes extremely large Neural Networks [44]. This chapter explains the principle of work behind deep learning and neural networks

2.2 Artificial Neural Networks [45]

Artificial neural networks (ANNs) have been a popular machine learning model since their introduction in the 1950s and have been extensively studied ever since. A neural network as shown in figure 2.1 consists roughly of several interconnected computational units called neurons that are arranged in layers. There is an input layer where data enters the network, followed by one or more hidden layers that transform the data as it flows through, and finally, an output layer where the neural network's predictions are generated. The network is trained to produce useful predictions by recognizing patterns in a set of labeled training data fed through it while an objective function compares the network's outputs with the actual labels. The network's parameters, which indicate the strength of each neuron, are modified throughout the training process until the patterns recognized by the network provide precise forecasts for the training data. After grasping the patterns, the network can anticipate new, previously unseen data by generalizing.

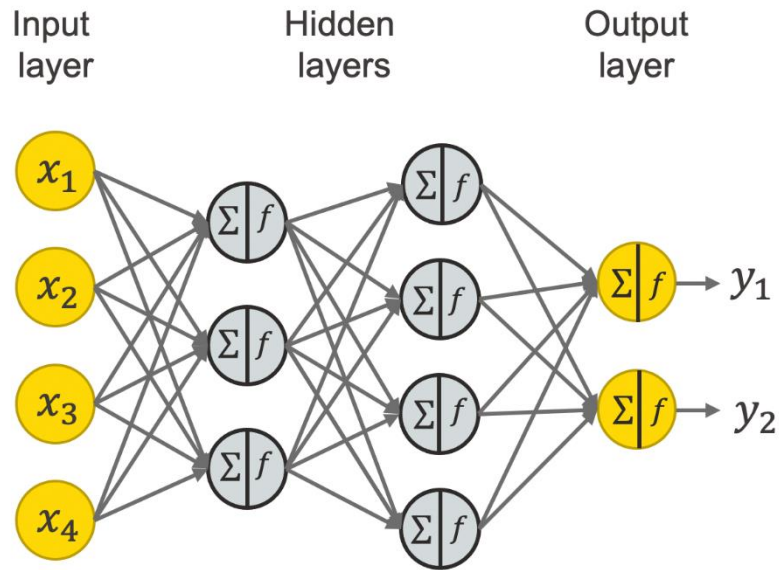


Figure 2. 1: neural network representation.

It has been known for a long time that ANNs are highly adaptable, and capable of modeling and solving complex problems, but also difficult and computationally expensive to train. This has diminished their practical utility, causing people to focus on other machine learning models until recently. Artificial neural networks are currently one of the most studied and dominant machine learning techniques. This transition is due to the growth of big data, powerful processors for parallel computations (particularly GPUs), key modifications to the algorithms used to construct and train the networks, and the development of simple software frameworks. Interest in ANNs is exploding, resulting in a rapid rate of innovation that is accelerating the development of other areas of machine learning. Simple linear functions are used to construct artificial neural networks, which are then followed by nonlinearities. The multilayer perceptron, or feedforward neural network, is one of the most

elementary types of neural network. Writing i for the i th layer and j for the j th unit of that layer, the output of the j th unit at the i th layer is:

$$z_j^{(i)} = \theta_j^{T(i)} x \quad (2.1)$$

Here, x consists of the previous layer's outputs that have been passed through a simple nonlinear function known as an activation function, typically a sigmoid function:

$$\sigma(z) = \frac{1}{1+e^{-x}} \quad (2.2)$$

or a rectified linear unit ReLU:

$$ReLU(z) = \max(0, z) \quad (2.3)$$

or small variations thereof. The network's layers perform computations by computing a weighted sum of the preceding layer's neuron outputs, followed by a nonlinearity. The resulting activations of each layer are then passed on to the next layer until the output layer, which produces the network's predictions. This process results in a hierarchical representation of the input data, where the earlier features tend to be more general and the output features become more specific. To train the network, training data is fed to the network, and the outputs and local derivatives at each node are recorded. The discrepancy between the output prediction and the true label is measured by an objective function, such as mean absolute error (L1), mean squared error (L2), cross-entropy loss, or Dice loss. The objective function's derivative with respect to the output is computed and used as feedback. The error is propagated backward through the network via backward propagation, which computes the gradient of the objective function with respect to the weights in each node using the chain rule

and dynamic programming. The weights are then adjusted using gradient descent, an optimization algorithm tasked with minimizing the error.

2.3 Deep Learning [45]–[47]

In traditional machine learning, models are trained by using manually engineered features extracted from raw data or features learned by other simple machine learning models to perform useful tasks. However, deep learning allows computers to automatically learn useful representations and features from raw data, which eliminates the need for this manual and tedious step. The fundamental similarity among deep learning techniques is their focus on feature learning, which refers to the automatic learning of data representations. This is the primary difference between deep learning and more conventional machine learning methods. Convolutional neural networks (CNNs) are the key driver of interest in deep learning as they are an extremely effective technique for learning useful representations of images and other structured data. Let's delve into the components of CNNs.

2.3.1 Building Blocks of Convolution Neural Network

While it is possible to use simple feedforward neural networks for image recognition, connecting all the nodes of one layer to all the nodes of the next can be highly inefficient. One solution is to trim connections based on domain knowledge, such as the structure of images, to improve performance. Convolutional neural networks (CNNs) are a specific type of artificial neural network that have been designed to preserve spatial relationships in data with a minimal number of connections between

layers. A typical CNN (shown in Figure 2.2) contains multiple convolutional and activation layers, often interspersed with pooling layers, and is trained using backpropagation and gradient descent, just like conventional neural networks. In addition, CNNs often include fully connected layers at the end to compute the final outputs. The efficiency of CNNs lies in their ability to produce highly effective data representations.

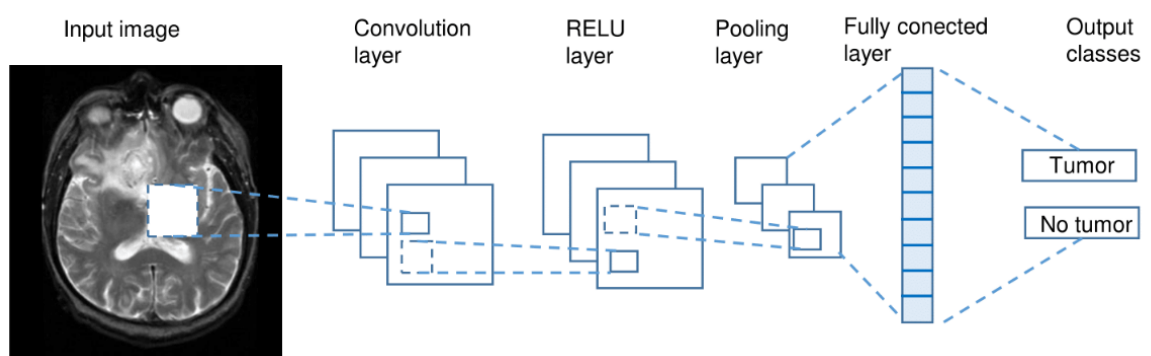


Figure 2. 2: typical convolutional neural network[48].

2.3.2 Convolutional Layer

The convolution operation involves two functions, namely an input function that consists of values (e.g., pixel values) at a particular position in an image and a filter (or kernel) function represented by an array of numbers. By computing the dot product of these two functions, an output is obtained. The filter is moved to the next position in the image according to the stride length, and the computation is repeated until the entire image is covered. This produces a feature map that highlights the regions where the filter is highly activated, indicating the presence of a specific feature, such as a line, a dot, or a curved edge. In the context of CNNs, when an image of a face is fed into the network, the initial filters detect low-level features, such as edges and lines, which are gradually combined

into increasingly complex features, like a nose, an eye, or an ear, as the feature maps serve as inputs for the next layer [48]. A convolutional layer comprises a set of learnable 2D filters, with each filter having a small spatial extent (width and height) but traversing the entire depth of the input feature. After applying convolution on the input and filters, the layer generates a feature map in two dimensions. Typically, a large number of learnable filters are employed to produce the output of the convolutional layer in three dimensions, H, W, and D, where H and W are the spatial dimensions, and D is the number of filters used. Equation 2.4 shows a discrete convolution in two dimensions with steps from (0, 0) to (m, n):

$$S(i, j) = \sum_m \sum_n K(m, n) I(i - m, j - n) \quad (2.4)[51]$$

Where:

S: the output.

I: the input image.

K: the kernel.

i,j: represents coordinates in the output feature map S.

(i-m,j-n): the coordinates in input I.

m,n: the coordinates in the kernel K.

Equation (2.5) is used to calculate the spatial dimension of the output, which is typically padded with zeros in order to maintain the input volume's spatial dimensions

$$W_{out} = \frac{W_{in} - K + 2P}{S} + 1 \quad (2.5)[51]$$

Where:

W_{out} : Output spatial dimension.

W_{in} : input spatial dimension.

K: kernel size.

S: stride.

P: zero padding.

Figure 2.3 depicts a convolutional layer with three 3x3 filters, stride $S = 1$, and padding size $P = 1$.

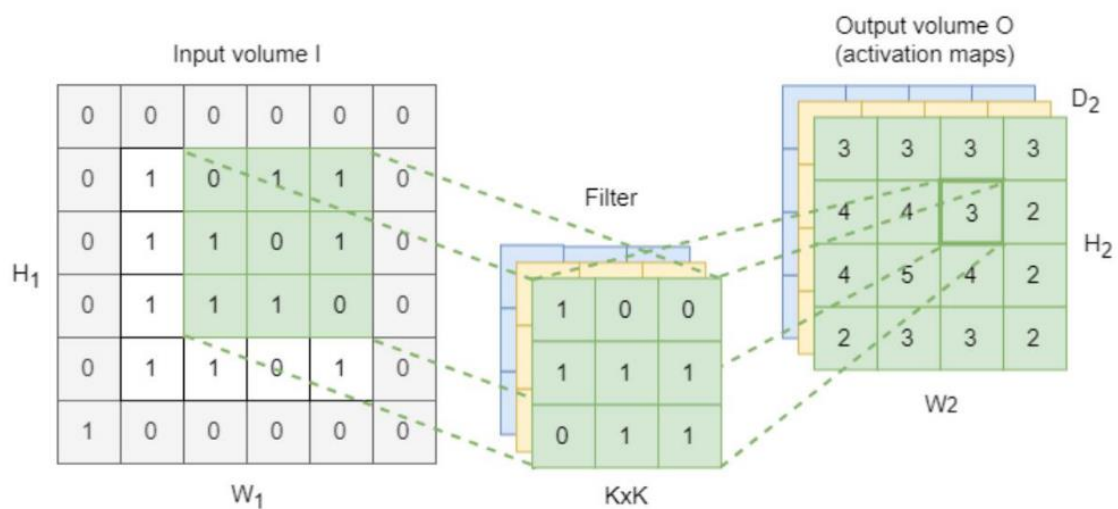


Figure 2. 3: Convolutional layer[52].

2.3.3 Activation Layer

Nonlinear activation functions are applied to the feature maps produced by a convolutional layer. This enables the neural network as a whole to approximate virtually any nonlinear function. The RELU is a popular activation function that converts negative input values to zero, as depicted in Figure 2.4. This simplifies and accelerates calculations and training, and prevents the vanishing gradient issue. It is defined mathematically as:

$$f(x) = \max(0, x) \quad (2.6)[48]$$

where x is the neuron's input. Sigmoid, Tanh, leaky RELUs, Randomized RELUs, and parametric RELUs are additional activation functions [48].

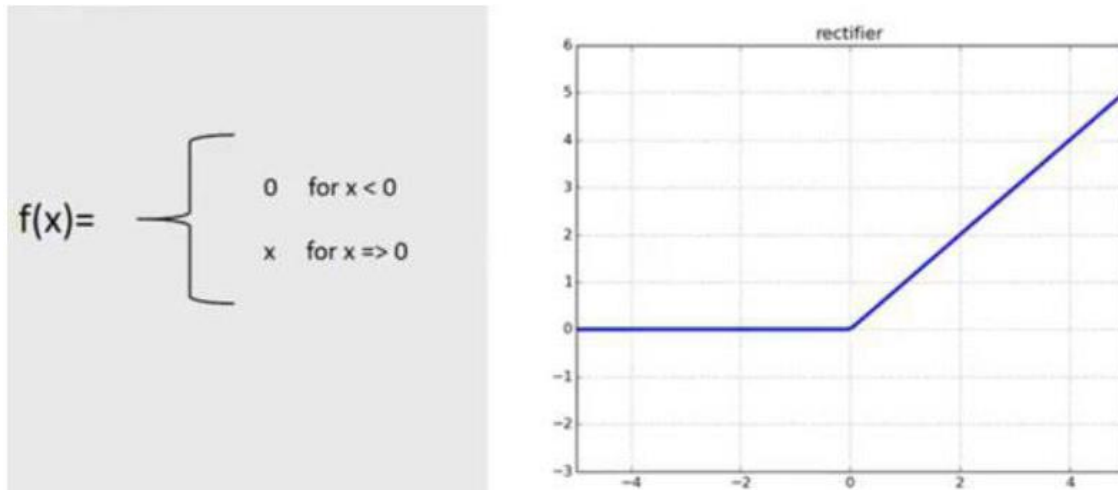
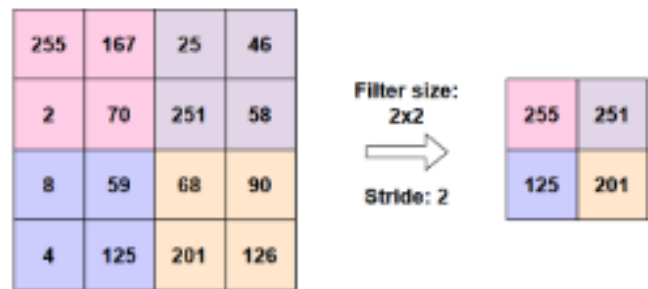


Figure 2. 4: ReLU activation function.

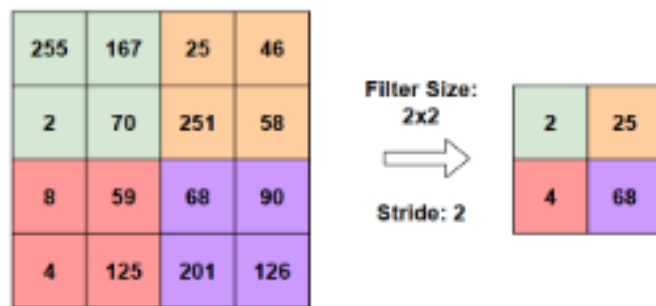
2.3.4 Pooling

The purpose of the pooling layer is to decrease the spatial dimensions of the convolved feature. By reducing the dimensionality of the data, less processing power is needed to process it. Moreover, it is beneficial to extract dominant features that are invariant to rotation and spatial orientation, which enables the model to be trained more [52]. There are three types of pooling: MAX pooling, MIN pooling, and average pooling. Max Pooling provides the maximum value from the kernel-covered region of the image, and is typically employed when the image has a dark background because it selects brighter pixels. In MIN pooling, the minimum value in a region represents the summary of the features in that region. Min pooling is typically employed when the image has a light background because it selects darker pixels. In contrast, Average Pooling calculates the mean of all the values within the kernel's region in the image, resulting in a smoothing effect that reduces sharp edges. It is

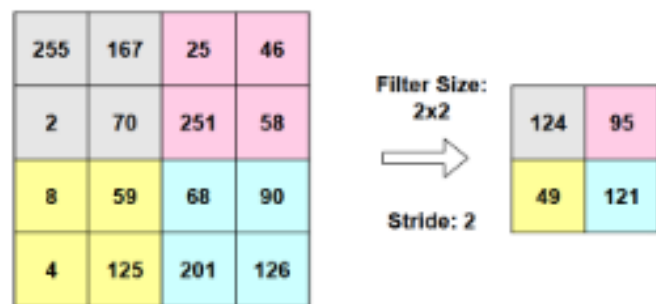
suitable for images where such edges are not essential [51]. figure 2.5 shows the operation.



MAX pooling



MIN pooling



Average pooling

Figure 2. 5: pooling operation with kernel size 2x2 and stride 2.

2.3.5 Batch Normalization

The training of Deep Neural Networks is complicated by the fact that the distribution of each layer's inputs changes as the parameters of the previous layers are modified. This slows down training by necessitating slower learning rates and more cautious initialization of parameters. This occurrence is referred to as an internal covariate shift. Batch normalization is a technique that speeds up neural networks and solves the internal covariate shift problem by adding additional layers to a deep neural network. The previous layer's input is normalized by the new layer [53].

2.3.6 Fully Connected Layer

The final layer of a convolutional neural network (CNN) is called the Fully Connected Layer, which is connected to every neuron in the preceding layer. The number of fully connected layers can vary depending on the level of feature abstraction required, similar to convolution, RELU, and pooling layers. The Fully Connected Layer takes the output of the preceding layer, whether Convolutional, RELU, or Pooling, and calculates a probability score for classification into different classes. In essence, this layer assesses the combination of the image's most highly activated features to identify its class [48].

3 Chapter three: Application of Deep Learning in Microwave Imaging System

3.1 Introduction

The objective of this study is to utilize deep learning techniques to analyze signals received by multiple antennas around the brain in order to detect the presence, size, and location of tumors. This chapter provides an overview of the workflow involved in achieving this goal. The steps involved in this study include:

1. Designing a microwave imaging system using six antennas placed around a head phantom with the aid of CST Studio Suite software.
2. Collecting an S-parameters dataset for various tumor sizes and locations inside the head.
3. Dividing the dataset into training and testing sets to ensure effective learning and evaluation.
4. Developing a Convolutional Neural Network (CNN) using MATLAB software.
5. Training the CNN with the training dataset.
6. Testing the ability of the CNN to detect tumors by evaluating it using the test dataset.

3.2 Microwave Imaging System

Figure 3.1 depicts the simulated Microwave Imaging (MWI) system developed using CST Studio Suite 2022. The system comprises six antipodal Vivaldi antennas and a Hugo head model, which is a pre-built head model within CST. The antennas are chosen for their wide bandwidth, directive radiation patterns, and ease of implementation in

CST. The antenna geometry is illustrated in Figure 3.2. The width (w) and length (l) of the antenna structure can be determined using Equations [54] provided the substrate's thickness (h), lowest operating frequency (f_l), and dielectric constant (ϵ_r) are known:

$$w = l = \frac{c}{f_l} \sqrt{\frac{2}{\epsilon_r + 1}} \quad (3.1)$$

$$r1 = \frac{w}{2} + \frac{w_m}{2} \quad (3.2)$$

$$r2 = \frac{w}{2} - \frac{w_m}{2} \quad (3.3)$$

$$rs1 = l + a \quad (3.4)$$

$$rs2 = 0.6r2 \quad (3.5)$$

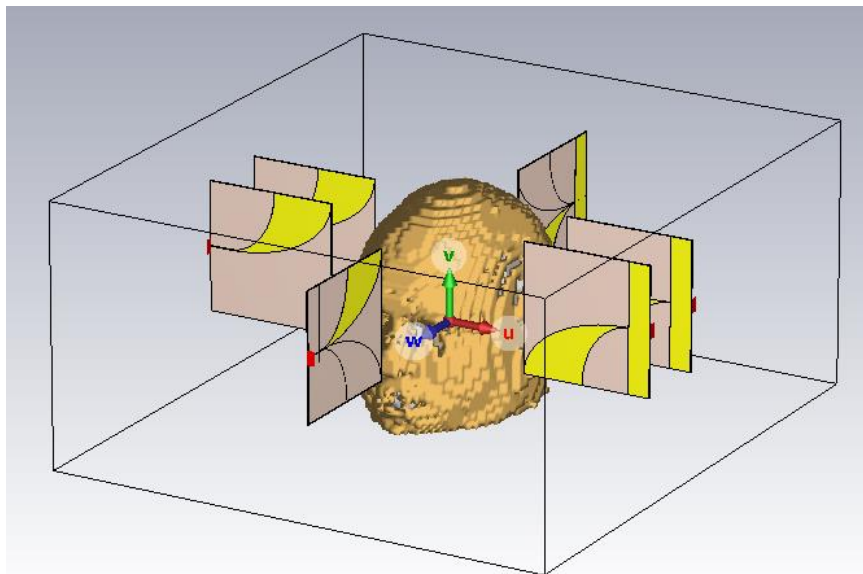


Figure 3. 1: Microwave Imaging system simulated in CST.

By utilizing these equations, the antenna structure's dimensions can be optimized for the desired frequency range and dielectric properties. This optimization process will ensure the optimal performance of the MWI system in detecting brain tumors with high accuracy.

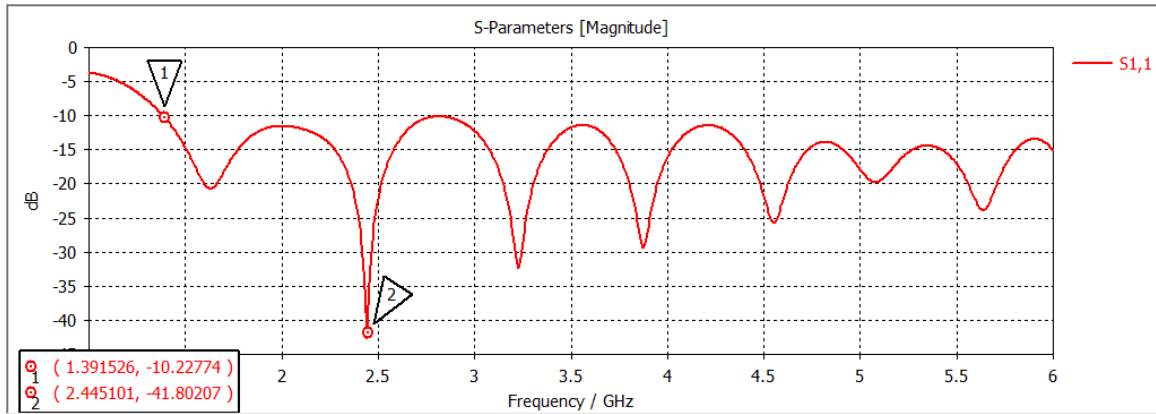


Figure 3. 3: $|S_{11}|$ of the designed antenna.

The simulated $|S_{11}|$ curve exhibits a significant decrease of -10 dB at 1.39 GHz, indicating the antenna's wideband characteristics. The curve also displays a resonance peak at 2.44 GHz, which confirms the antenna's suitability for operating in this frequency range. Furthermore, Figure 3.4 illustrates the directive far-field radiation pattern of the antenna, which has a maximum gain of 8 dB.

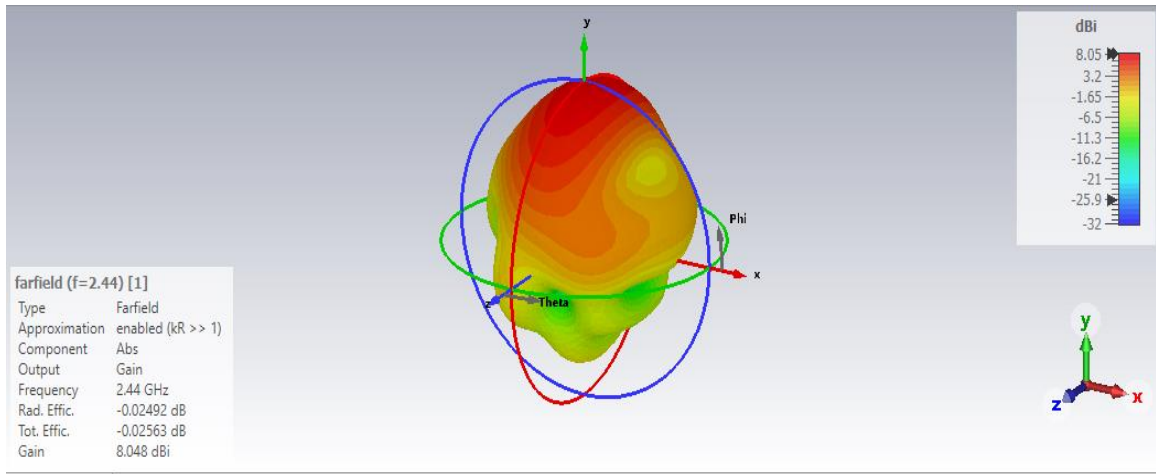


Figure 3. 4: far filed radiation pattern of the antenna.

The CST software provides various readily available bio models for the head. Figure 3.5 illustrates the head model (HUGO) with 16 different tissues. To characterize the dielectric properties of the head tissues, a

frequency of 2.44 GHz was used, which is the resonance frequency of the antenna. To optimize computation time, only six tissues, namely bone cortical, brain grey matter, brain white matter, cerebellum, fat, and skin were selected. The head phantom had dimensions of 174 mm in width (x-direction), 227 mm in length (z-direction), and 100 mm in height (y-direction). The system consisted of six antennas positioned 15 mm from the head. A spherical malignant tumor was inserted into the head phantom with a relative permittivity of 62 and a tangent loss of 0.594 at 2.44 GHz as illustrated in figure 3.6 [2].

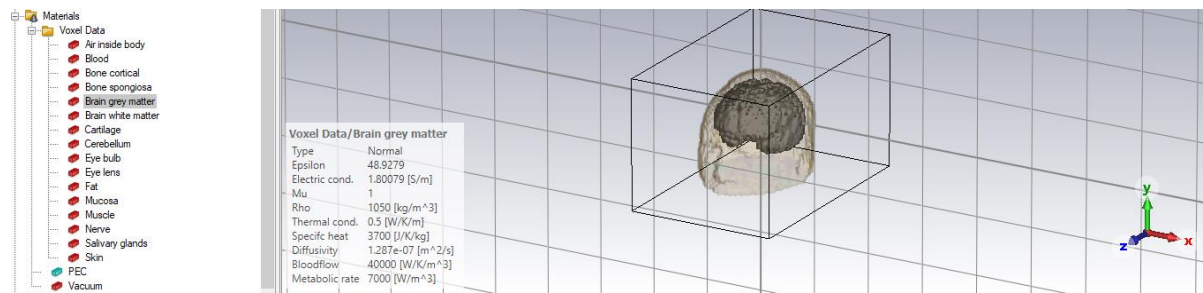


Figure 3. 5: tissues of the voxel head model (HUGO) in CST.

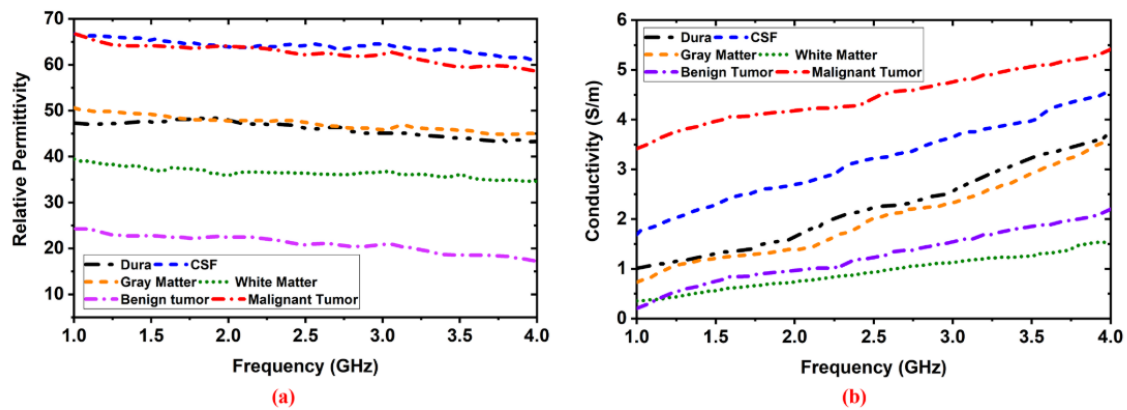


Figure 3. 6: dielectric properties of head tissues. (a) permittivity, (b) conductivity.

3.3 Dataset Construction and Generation

In order to train a neural network to detect the existence, size, and location of tumors, a diverse dataset of tumors with varying sizes and

locations is required. For this study, a dataset of 628 scans was used, which included 308 scans with tumors of 11 different sizes placed at 28 different locations in the x-z plane (4 points in x-direction and 7 points in z-direction) at y=60 mm. In order to create scans without tumors, a small tumor of radius 0.0001 mm was used in 320 different locations in the x-z plane (18 points in x-direction and 21 points in z-direction) at y=60 mm. Tables 3.1 and 3.2 summarize the specific points that were included in the dataset, with all dimensions given in millimeters and the radius of the spherical tumor denoted as (r).

Table 3. 1 tumor-exist scans

	Existence	Size (r)	x	y	z
1	Yes	0.2	-45	60	-70
2		0.4	-15		-50
3		0.6	15		-20
4		0.8	45		0
5		1			15
6		2			35
7		4			50

8		6			
9		8			
10		10			
11		12			
Total	308 cases	11	4	1	7

Table 3. 2 tumor-non exist scans

	Existence	Size (r)	x	y	z
1	No	0.0001	-45	60	-60
2			-40.5		-54
3			-36		-48
4			-31.5		-42
5			-27		-36
6			-22.5		-30
7			-18		-24

8			-13.5		-18
9			-9		-12
10			-4.5		-6
11			0		0
12			4.5		6
13			9		12
14			13.5		18
15			18		24
16			22.5		30
17			27		36
18			31.5		42
19					48
20					45
21					60
Total	320 case	1	18	1	21

Each scan was imaged by 6 antennas around the head, this produces 36 s-parameter (s_{11} , s_{21}, s_{66}) per each scan. 1001 samples were taken from a frequency span from 1.5 to 4.5 GHz of the measured s-parameters. Each s-parameter channel has a magnitude and phase. The data is arranged in a 4-D matrix of 36 (channel) x 1001 (samples) x 2 (magnitude and phase) x 628 (scan). For simplicity of training, each problem of detecting the existence, size, and the location in x-z plane is dealt with solely.

3.4 Training Methods

3.4.1 Training a Convolution Neural Network (CNN) to Detect the Existence of Tumors

MATLAB 2021b was used. First, the dataset of $36 \times 1001 \times 2 \times 628$ was normalized and randomly permuted. Then the dataset was divided into a training set of 500 scans which is used to train the network, and a test set of 128 scans which are used to test the ability of the network to generalize well to unseen data. the CNN architecture was:

- Input layer ($36 \times 1001 \times 2$).
- Convolutional layer (12 filters, each of size $3 \times 3 \times 2$).
- Relu activation function.
- Dense output layer (2 neurons, one for each class).
- Softmax activation function (this function gives the probability that a given class appears).

With the cross-entropy cost function, the network was trained by the Adam optimizer with the following parameters:

Table 3. 3 Parameters of the training to predict the existence of the tumor

Parameter	Value
Learning rate	0.0001
Batch size	128
Learning rate drop period	50
Learning rate drop factor	0.65
Regularization parameter	0.0001

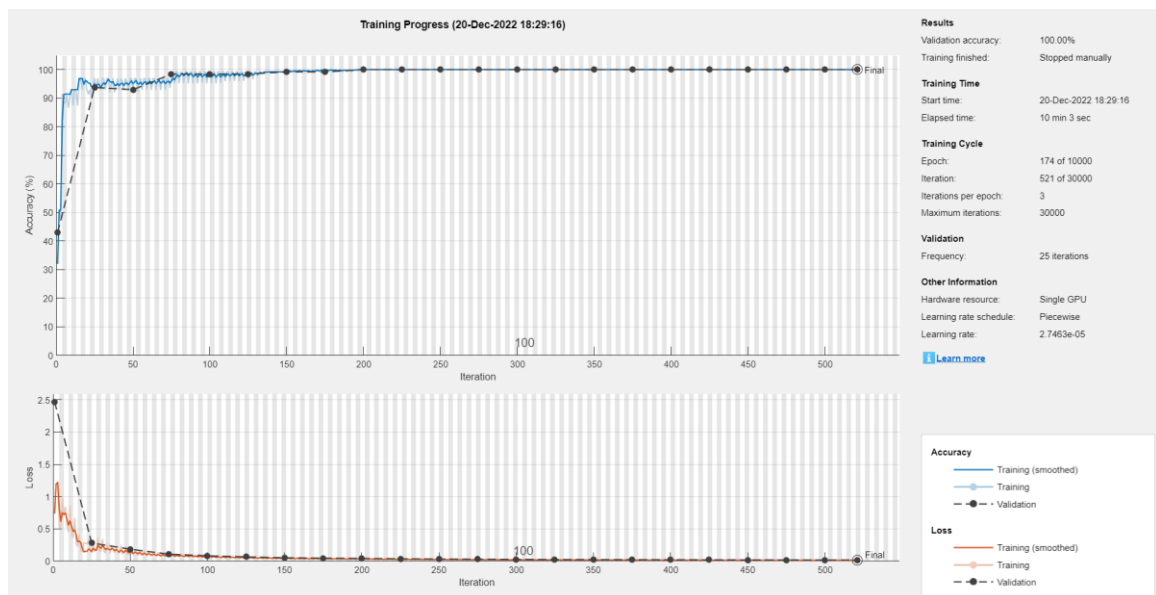


Figure 3. 7: training/testing loss/accuracy curves of the CNN that detect the existence of tumors.

The training progress of the neural network is shown in Figure 3.7, which displays the accuracy and loss of the network across training iterations. The loss metric indicates the degree to which the network's predictions deviate from the true values, and it was observed to decrease as expected over the course of training. Similarly, the accuracy metric, which measures the proportion of correct classifications, showed an expected increase over time, suggesting successful training. After 174 epochs, both the training and validation (test data) accuracy reached 100%, indicating that the network had learned a strong relationship between the raw data of the s-parameters and the presence of tumors. Furthermore, the network was able to classify unseen data with perfect accuracy, which is a highly promising result..

3.4.2 Training a Convolution Neural Network (CNN) to Predict the Size of the Tumor

To train the network to predict the size of the tumor, only the tumor-exist data is needed which is in the form of $36 \times 1001 \times 2 \times 308$. As was done before the 308 scan data was normalized and randomly permuted. Then it was divided into 250 scan trainsets and 48 scan test sets. the CNN architecture was:

- Input layer ($36 \times 1001 \times 2$).
- Convolutional layer (12 filters, each of size $3 \times 3 \times 2$).
- Relu activation function.
- Dense output layer (one neuron)

With the mean squared error MSE as the cost function, The network was also trained with Adam optimizer with the following parameters:

Table 3. 4 parameters of the training to predict the size of the tumor

Parameter	Value
Learning rate	0.0001
Batch size	128
Learning rate drop period	200
Learning rate drop factor	0.65
Regularization parameter	1

Notice that in problems where the neural network has to predict continuous values like the size, The root mean squared error (RMSE) is considered to represent the accuracy because it represents how much the predicted value deviates from the true value and should be decreased as the training progresses.

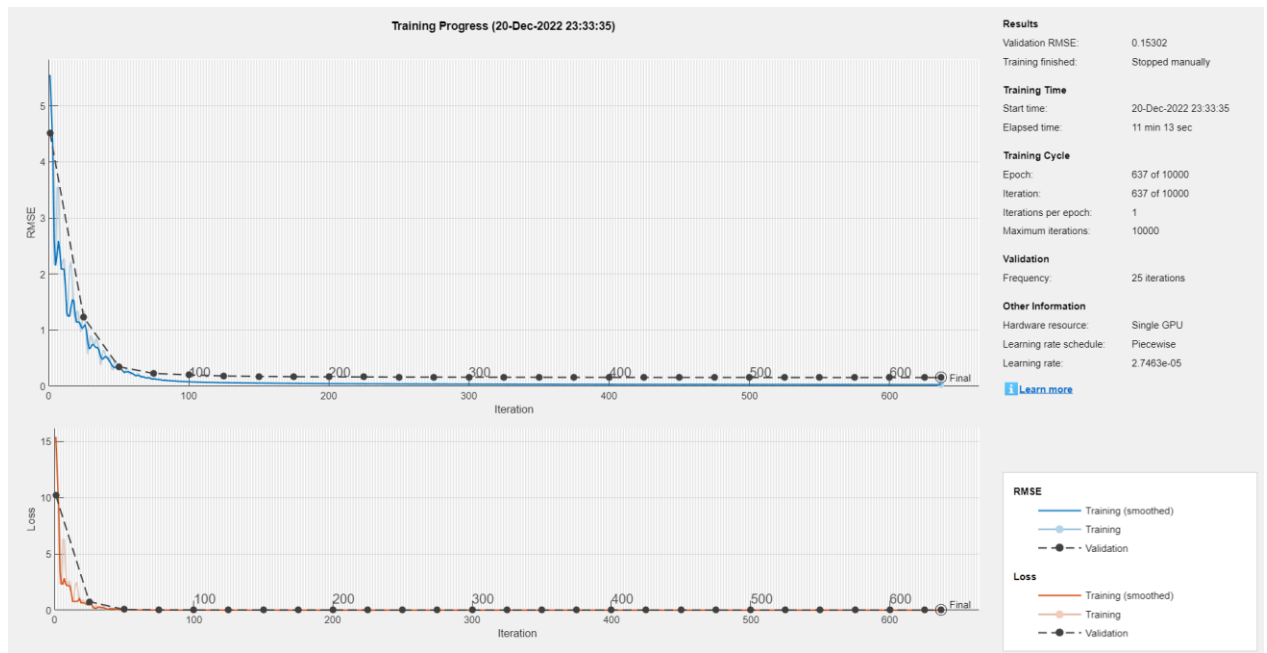


Figure 3. 8: training/testing loss /RMSE of a CNN that predicts the size of the tumor.

The training progress of the neural network is shown in Figure 3.8, where both the root mean squared error (RMSE) and the loss start at high values and gradually decrease as the training proceeds, indicating that the training is progressing as expected. After 637 epochs, the test RMSE and training RMSE were measured at 0.15 mm and 0.03 mm, respectively. These values suggest that the network has learned a relationship between the raw data s-parameter and the radius (r) of the tumor, and is able to generalize to unseen data with good or acceptable average error.

3.4.3 Training a Convolution Neural Network (CNN) to Predict the Location of the Tumor in the x-z Plane

The 308 scans were divided into 280 train sets, and 28 test set. The following CNN architecture was used:

- Input (36x1001x2).
- Convolutional layer (12 filters, each of size 3x3x2).

- Relu activation function.
- Dense layer (5 neurons)
- Softplus activation function
- Dense output layer (one neuron)

The cost function is MSE, and the network was again trained by Adam optimizer with the following parameters:

Table 3. 5 parameters of the training to predict the location

Parameter	Value
Learning rate	0.0001
Batch size	128
Learning rate drop period	200
Learning rate drop factor	0.65
Regularization parameter	0.0001

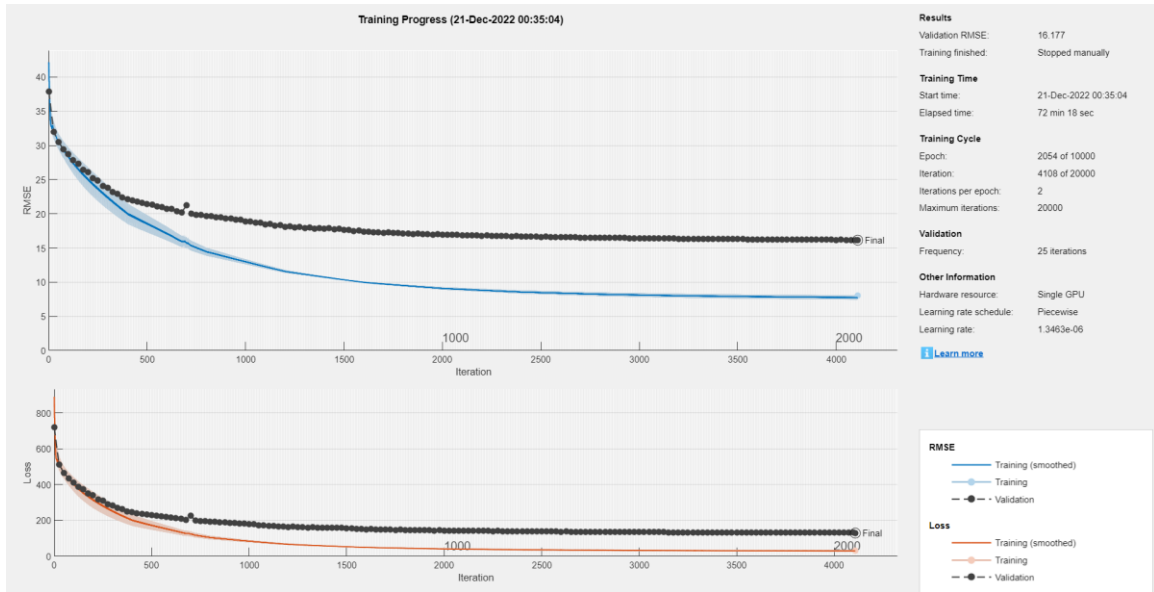


Figure 3. 9: training/testing loss /RMSE of a CNN that predicts the z-direction of the tumor.

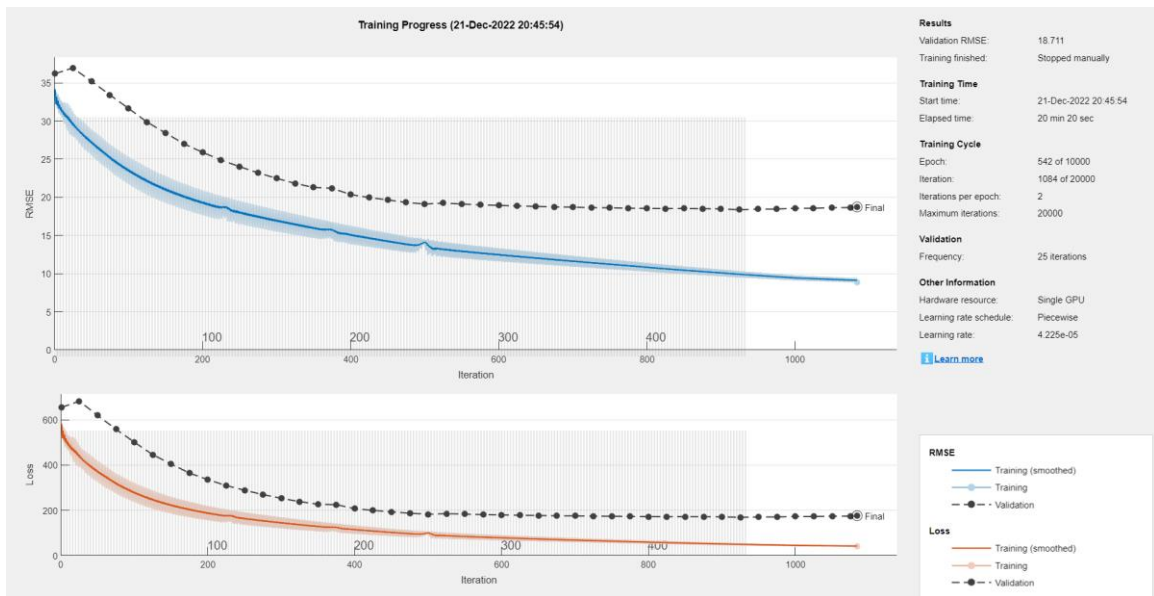


Figure 3. 10 training/testing loss /RMSE of a CNN that predicts the x-direction of the tumor.

As seen in figures 3.9 and 3.10, The relatively wide difference between the training RMSE and test RMSE indicates that the model may overfit the training data (overfit: a case where the network can learn relationship on the trainset but fails to generalize to unseen data the test set). This may be due to the small amount of location data, (only 7 points

in the z-direction and 4 points in a span of almost 150 mm in the z-direction and 100 mm in the x-direction), and getting more data is likely help to enhance the generalization of the model. To check this a convolutional neural network was trained on the tumor-non exist data to detect the location, since this dataset has more points in z and x directions (21 points in z and 18 points in x). the 320 scans were divided into 280 scan train set and 40 scan test set. the CNN architecture was:

- Input layer (36x1001x2).
- Convolutional layer (12 filters, each of size 3x3x2).
- Relu activation function.
- Dense output layer (one neuron)

The cost function is MSE, and the network was trained by Adam optimizer with the following parameters:

Table 3. 6 parameters of the training to predict the location using tumor-non exist data

Parameter	Value
Learning rate	0.0004
Batch size	128
Learning rate drop period	125
Learning rate drop factor	0.65

Regularization parameter

0.1

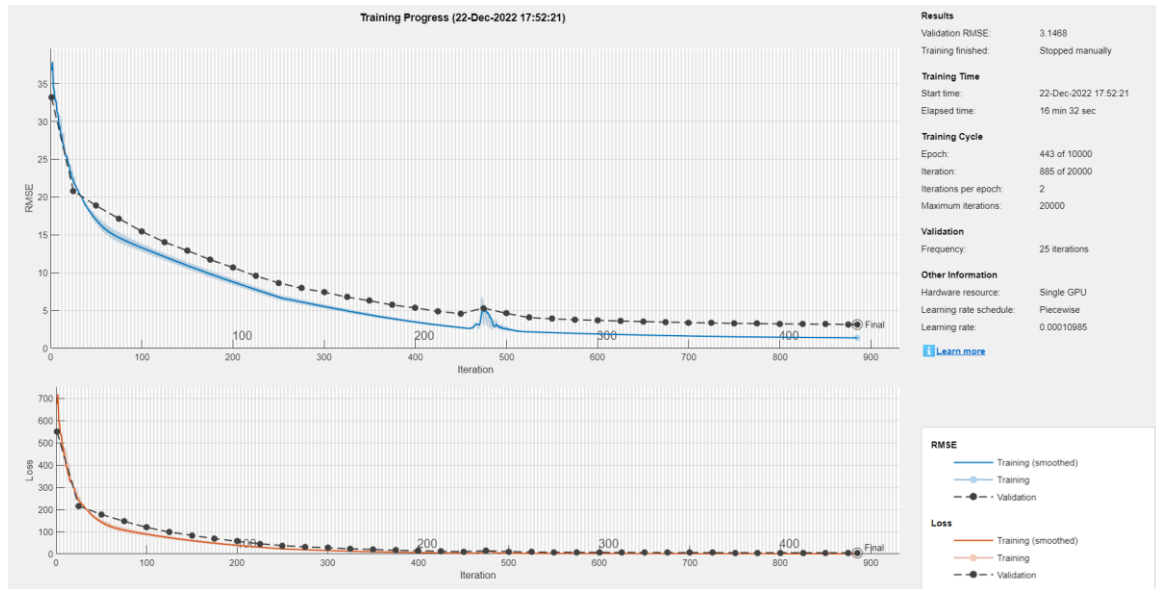


Figure 3. 11: training/testing loss /RMSE of a CNN that predicts the z-direction of the tumor-non exist dataset.

After 443 epochs the training and validation RMSE were 1.5,3.14 mm, this close and relatively small value indicates that the network learned a relationship between s-parameter data and was able to generalize well. The more data in the tumor-non exist dataset allowed the network generalization to be better.

4 Chapter 4: Conclusion and Future Work

4.1 Conclusion

This study investigated the capability of using deep learning to detect the existence, size, and location of brain tumors from the raw electromagnetic data gathered from a microwave imaging system consisting of 6 antennas around the head. The following findings can be drawn:

1. The antipodal Vivaldi antenna is suitable for investigating the microwave imaging system and machine learning application as it is simple to design, offers wide bandwidth(1.39GHz-6GHz), and has a suitable gain of 8 dBi.
2. The use of Six antennas around the head in the microwave imaging system over frequency band of 1.5 to 4.5 GHz is feasible as a starting point.
3. A convolutional neural network (CNN) of 12 filters of size 3x3 with relu activation function can be trained to detect the presence of tumors from the raw electromagnetic data and was able to classify unseen tumors data as small tumors as 0.2 mm radius at the accuracy of 100%.
4. A CNN of 12 filters of size 3x3 with relu activation function can be trained to predict the size of the tumors from the raw electromagnetic and was able to predict the radius of unseen tumors data with average deviation from the true size of 0.15 mm (RMSE).

5. A CNN 12 filter of size 3x3 with relu activation function can be trained to predict the location of the tumors from the raw electromagnetic data and was able to predict the location in z-coordinate of unseen tumors data with average deviation from the true location of 3.14 mm.
6. using 308 tumor-exist scans (11 sizes in 28 locations in the x-z plane) and 320 tumor-non exist scans (a tumor of the size of 0.0001 mm in 320 locations was assumed) was acceptable to get the CNN to be trained to detect the presence of tumors and generalize to unseen data.
7. Using 11 tumor sizes of (0.2,0.4,0.6,0.8,1,2,4,6,8,10,12) mm in 28 different locations in the x-z plane was acceptable to get the CNN to be trained to determine the radius of the tumors and generalize to unseen data.
8. Using 7 tumor locations in the z-direction of (-70, -50, -20,0,15,35,50) mm and 4 points in the x-direction of (-45, -15,15,45) led the CNN to overfit the training data (fails to generalize to unseen data). And this could be due to the large step size. Using the tumor-non exist scans to train the CNN to predict the location in the z-direction was acceptable to get the network to generalize to unseen data. this is because tumor-non exist scans has rich location data (21 point in z and 18 points in x).

This study highlights the importance of having sufficient and appropriate data for training deep neural networks, which can then

achieve remarkable accuracy in detecting brain tumors from raw electromagnetic data.

4.2 Future Work

For future work, one can take into consideration the following:

1. Classifying the type of the tumor whether it's malignant or benign.
2. Finding the location in 3D.
3. Use all the tissues in the head in the simulation.

References

- [1] "Cancer." https://www.who.int/health-topics/cancer#tab=tab_1 (accessed Aug. 15, 2022).
- [2] A. Hossain, M. T. Islam, and A. F. Almutairi, "A deep learning model to classify and detect brain abnormalities in portable microwave based imaging system," *Sci. Rep.*, vol. 12, no. 1, pp. 1–27, 2022, doi: 10.1038/s41598-022-10309-6.
- [3] A. Dna, "Brain and Spinal Cord Tumors in Adults," *Am. Cancer Soc.*, pp. 1–49, 2011.
- [4] Cancer.Net Editorial Board, "Brain Tumor: Statistics | Cancer.Net," 2016. <https://www.cancer.net/cancer-types/brain-tumor/statistics> (accessed Aug. 15, 2022).
- [5] A. Dna, "Brain and Spinal Cord Tumors in Adults," *Am. Cancer Soc.*, vol. 103, no. 2, pp. 1–49, 2011.
- [6] "Brain Tumor FAQs - Learn More or Donate Today! | ABTA." <https://www.abta.org/about-brain-tumors/brain-tumor-education/> (accessed Aug. 15, 2022).
- [7] N. B. Bahadure, A. K. Ray, and H. P. Thethi, "Image Analysis for MRI Based Brain Tumor Detection and Feature Extraction Using Biologically Inspired BWT and SVM," *Int. J. Biomed. Imaging*, vol. 2017, 2017, doi: 10.1155/2017/9749108.
- [8] A. T. Mobashsher, "Wideband Microwave Imaging System for Brain Injury Diagnosis," *Phd Thesis Univ. Qld.*, 2016.
- [9] A. Hossain *et al.*, "A YOLOv3 Deep Neural Network Model to Detect Brain Tumor in Portable Electromagnetic Imaging System," *IEEE Access*, vol. 9, pp. 82647–82660, 2021, doi: 10.1109/ACCESS.2021.3086624.
- [10] A. Salleh, C. Chiou, T. Alam, M. Singh, J. Singh, and M. Tariqul, "Development of Microwave Brain Stroke Imaging System using Multiple Antipodal Vivaldi Antennas Based on Raspberry Pi Technology," *J. Eng.*, vol. 32, no. 1, pp. 39–49, 2020, doi: 10.17576/jkukm-2020-32(1)-06.
- [11] M. Nazir, S. Shakil, and K. Khurshid, "Role of deep learning in brain tumor detection and classification (2015 to 2020): A review," *Comput. Med. Imaging Graph.*, vol. 91, no. May, 2021, doi: 10.1016/j.compmedimag.2021.101940.
- [12] W. Shao and T. Mccollough, "Advances in Microwave Near-Field Imaging," *IEEE Microw. Mag.*, no. May, pp. 94–119, 2020.
- [13] R. Chandra, H. Zhou, I. Balasingham, and R. M. Narayanan, "On the Opportunities and Challenges in Microwave Medical Sensing and Imaging," *IEEE Trans. Biomed. Eng.*, vol. 62, no. 7, pp. 1667–1682, 2015, doi: 10.1109/TBME.2015.2432137.
- [14] J. C. Lin and M. J. Clarke, "Microwave Imaging of Cerebral Edema," *Proc. IEEE*, vol. 70, no. 5, pp. 523–524, 1982, doi: 10.1109/PROC.1982.12341.
- [15] H. Trefná and M. Persson, "Antenna array design for brain monitoring," *2008 IEEE Int. Symp. Antennas Propag. Usn. Natl. Radio Sci. Meet. APSURSI*, 2008, doi: 10.1109/APS.2008.4619683.

- [16] S. Y. Semenov and D. R. Corfield, "Microwave Tomography for Brain Imaging: Feasibility Assessment for Stroke Detection," *Int. J. Antennas Propag.*, vol. 2008, pp. 1–8, 2008, doi: 10.1155/2008/254830.
- [17] S. Semenov, B. Seiser, E. Stoegmann, and E. Auff, "Electromagnetic tomography for brain imaging: From virtual to human brain," *2014 IEEE Conf. Antenna Meas. Appl. CAMA 2014*, Jan. 2014, doi: 10.1109/CAMA.2014.7003417.
- [18] S. Semenov *et al.*, "Electromagnetic tomography for brain imaging: Initial assessment for stroke detection," *IEEE Biomed. Circuits Syst. Conf. Eng. Healthy Minds Able Bodies BioCAS 2015 - Proc.*, Dec. 2015, doi: 10.1109/BIOCAS.2015.7348385.
- [19] M. Persson *et al.*, "Microwave-based stroke diagnosis making global prehospital thrombolytic treatment possible," *IEEE Trans. Biomed. Eng.*, vol. 61, no. 11, pp. 2806–2817, Nov. 2014, doi: 10.1109/TBME.2014.2330554.
- [20] A. Fhager and M. Persson, "A microwave measurement system for stroke detection," *LAPC 2011 - 2011 Loughb. Antennas Propag. Conf.*, 2011, doi: 10.1109/LAPC.2011.6114001.
- [21] S. Candefjord *et al.*, "Microwave technology for detecting traumatic intracranial bleedings: tests on phantom of subdural hematoma and numerical simulations," *Med. Biol. Eng. Comput.*, vol. 55, no. 8, pp. 1177–1188, Aug. 2017, doi: 10.1007/S11517-016-1578-6/FIGURES/9.
- [22] J. Ljungqvist, S. Candefjord, M. Persson, L. Jönsson, T. Skoglund, and M. Elam, "Clinical Evaluation of a Microwave-Based Device for Detection of Traumatic Intracranial Hemorrhage," *J. Neurotrauma*, vol. 34, no. 13, pp. 2176–2182, Jul. 2017, doi: 10.1089/NEU.2016.4869.
- [23] A. Ghaaliq, L. Mb, C. Frca, A. Mccluskey, and B. Mb, "Clinical tests: sensitivity and specificity," *Contin. Educ. Anaesth. Crit. Care Pain*, vol. 8, no. 6, pp. 221–223, Dec. 2008, doi: 10.1093/BJACEACCP/MKN041.
- [24] M. Jalilvand, T. Zwick, W. Wiesbeck, and E. Pancera, "UWB synthetic aperture-based radar system for hemorrhagic head-stroke detection," *IEEE Natl. Radar Conf. - Proc.*, pp. 956–959, 2011, doi: 10.1109/RADAR.2011.5960677.
- [25] H. Zhang, B. Flynn, A. T. Erdogan, and T. Arslan, "Microwave imaging for brain tumour detection using an UWB Vivaldi Antenna array," *LAPC 2012 - 2012 Loughb. Antennas Propag. Conf.*, 2012, doi: 10.1109/LAPC.2012.6402964.
- [26] B. J. Mohammed, A. M. Abbosh, and D. Ireland, "Stroke detection based on variations in reflection coefficients of wideband antennas," *IEEE Antennas Propag. Soc. AP-Int. Symp. Dig.*, 2012, doi: 10.1109/APS.2012.6348795.
- [27] B. J. Mohammed, A. M. Abbosh, S. Mustafa, and D. Ireland, "Microwave system for head imaging," *IEEE Trans. Instrum. Meas.*, vol. 63, no. 1, pp. 117–123, Jan. 2014, doi: 10.1109/TIM.2013.2277562.
- [28] A. T. Mobashsher and A. M. Abbosh, "Compact 3-D Slot-Loaded Folded Dipole Antenna with Unidirectional Radiation and Low Impulse Distortion for Head Imaging

Applications,” *IEEE Trans. Antennas Propag.*, vol. 64, no. 7, pp. 3245–3250, Jul. 2016, doi: 10.1109/TAP.2016.2560909.

[29] A. T. Mobashsher, A. M. Abbosh, and Y. Wang, “Microwave system to detect traumatic brain injuries using compact unidirectional antenna and wideband transceiver with verification on realistic head phantom,” *IEEE Trans. Microw. Theory Tech.*, vol. 62, no. 9, pp. 1826–1836, 2014, doi: 10.1109/TMTT.2014.2342669.

[30] A. T. Mobashsher, B. J. Mohammed, S. Mustafa, and A. Abbosh, “Ultra wideband antenna for portable brain stroke diagnostic system,” *2013 IEEE MTT- Int. Microw. Workshop Ser. RF Wirel. Technol. Biomed. Healthc. Appl. IMWS-BIO 2013 - Proc.*, 2013, doi: 10.1109/IMWS-BIO.2013.6756163.

[31] A. T. Mobashsher and A. Abbosh, “Development of compact directional antenna utilising plane of symmetry for wideband brain stroke detection systems,” *Electron. Lett.*, vol. 50, no. 12, pp. 850–851, Jun. 2014, doi: 10.1049/EL.2014.0616.

[32] A. T. Mobashsher and A. M. Abbosh, “Three-dimensional human head phantom with realistic electrical properties and anatomy,” *IEEE Antennas Wirel. Propag. Lett.*, vol. 13, pp. 1401–1404, 2014, doi: 10.1109/LAWP.2014.2340409.

[33] A. T. Mobashsher and A. M. Abbosh, “On-site Rapid Diagnosis of Intracranial Hematoma using Portable Multi-slice Microwave Imaging System,” *Sci. Rep. 2016 61*, vol. 6, no. 1, pp. 1–17, Nov. 2016, doi: 10.1038/srep37620.

[34] A. E. Stancombe, K. S. Bialkowski, and A. M. Abbosh, “Portable microwave head imaging system using software-defined radio and switching network,” *IEEE J. Electromagn. RF Microw. Med. Biol.*, vol. 3, no. 4, pp. 284–291, Dec. 2019, doi: 10.1109/JERM.2019.2901360.

[35] M. S. R. Bashri, “Wearable Devices for Microwave Head Diagnostic Systems,” 2018.

[36] A. S. M. Alqadami, K. S. Bialkowski, A. T. Mobashsher, and A. M. Abbosh, “Wearable Electromagnetic Head Imaging System Using Flexible Wideband Antenna Array Based on Polymer Technology for Brain Stroke Diagnosis,” *IEEE Trans. Biomed. Circuits Syst.*, vol. 13, no. 1, pp. 124–134, Feb. 2019, doi: 10.1109/TBCAS.2018.2878057.

[37] M. S. R. Bashri, T. Arslan, W. Zhou, and N. Haridas, “Wearable device for microwave head imaging,” *Eur. Microw. Week 2016 Microw. Everywhere EuMW 2016 - Conf. Proc. 46th Eur. Microw. Conf. EuMC 2016*, pp. 671–674, 2016, doi: 10.1109/EUMC.2016.7824432.

[38] W. Shao and Y. Du, “Microwave Imaging by Deep Learning Network: Feasibility and Training Method,” *IEEE Trans. Antennas Propag.*, vol. 68, no. 7, pp. 5626–5635, 2020, doi: 10.1109/TAP.2020.2978952.

[39] A. Yago, M. Cavagnaro, and L. Crocco, “Deep Learning-Enhanced Qualitative Microwave Imaging: Rationale and Initial Assessment,” *15th Eur. Conf. Antennas Propag. EuCAP 2021*, Mar. 2021, doi: 10.23919/EUCAP51087.2021.9411361.

[40] N. M. Dipu, S. A. Shohan, and K. M. A. Salam, “Deep Learning Based Brain Tumor Detection and Classification,” *2021 Int. Conf. Intell. Technol. CONIT 2021*, Jun. 2021, doi: 10.1109/CONIT51480.2021.9498384.

- [41] E. Avşar and K. Salçin, "Detection and classification of brain tumours from MRI images using faster R-CNN," *Teh. Glas.*, vol. 13, no. 4, pp. 337–342, Dec. 2019, doi: 10.31803/TG-20190712095507.
- [42] H. Dong, G. Yang, F. Liu, Y. Mo, and Y. Guo, "Automatic brain tumor detection and segmentation using U-net based fully convolutional networks," *Commun. Comput. Inf. Sci.*, vol. 723, pp. 506–517, 2017, doi: 10.1007/978-3-319-60964-5_44/COVER.
- [43] Y. Baştanlar and M. Ozuysal, *Introduction to Machine Learning Second Edition*, vol. 1107. 2014. doi: 10.1007/978-1-62703-748-8_7.
- [44] I. H. Sarker, "Machine Learning: Algorithms, Real-World Applications and Research Directions," *SN Comput. Sci.*, vol. 2, no. 3, pp. 1–21, 2021, doi: 10.1007/s42979-021-00592-x.
- [45] A. S. Lundervold and A. Lundervold, "An overview of deep learning in medical imaging focusing on MRI," *Z. Med. Phys.*, vol. 29, no. 2, pp. 102–127, 2019, doi: 10.1016/j.zemedi.2018.11.002.
- [46] M. Griebel, A. Dürr, and N. Stein, "Applied Image Recognition: Guidelines for using Deep Learning Models in Practice," *Proc. 14th Int. Conf. Wirtsch.*, pp. 393–406, 2019.
- [47] J. Ker, L. Wang, J. Rao, and T. Lim, "Deep Learning Applications in Medical Image Analysis," *IEEE Access*, vol. 6, no. c, pp. 9375–9379, 2017, doi: 10.1109/ACCESS.2017.2788044.
- [48] J. Ker, L. Wang, J. Rao, and T. Lim, "Deep Learning Applications in Medical Image Analysis," *IEEE Access*, vol. 6, pp. 9375–9379, 2017, doi: 10.1109/ACCESS.2017.2788044.
- [49] M. Lin, Q. Chen, and S. Yan, "Network In Network," *2nd Int. Conf. Learn. Represent. ICLR 2014 - Conf. Track Proc.*, Dec. 2013, doi: 10.48550/arxiv.1312.4400.
- [50] Y. Lecun, Y. Bengio, and G. Hinton, "Deep learning," *Nat. 2015 5217553*, vol. 521, no. 7553, pp. 436–444, May 2015, doi: 10.1038/nature14539.
- [51] J. N. Slettevold, "Deep learning in Dynamic Imager - A convolutional neural network module," 2018.
- [52] V. N. Nguyen, R. Jenssen, and D. Roverso, "Automatic autonomous vision-based power line inspection: A review of current status and the potential role of deep learning," *Int. J. Electr. Power Energy Syst.*, vol. 99, pp. 107–120, Jul. 2018, doi: 10.1016/J.IJEPES.2017.12.016.
- [53] S. Ioffe and C. Szegedy, "Batch Normalization: Accelerating Deep Network Training by Reducing Internal Covariate Shift," *32nd Int. Conf. Mach. Learn. ICML 2015*, vol. 1, pp. 448–456, Feb. 2015, doi: 10.48550/arxiv.1502.03167.
- [54] A. M. Abbosh, H. Kan, and M. E. Bialkowski, "Design of compact directive ultra wideband antipodal antenna," *Microw. Opt. Technol. Lett.*, vol. 48, Dec. 2006, doi: 10.1002/mop.21955.
- [55] I. Bulu and H. Caglayan, "DESIGNING MATERIALS WITH DESIRED," *Microw. Opt.*, vol. 48, no. 12, pp. 2611–2615, 2006, doi: 10.1002/mop.

الخلاصة

من أكبر المشاكل في عالم الطب وجود الأورام وخاصة في الدماغ. الكشف المبكر عن الورم هو مفتاح العلاج الناجح. تقنيات التصوير الطبي الحالية ، مثل التصوير المقطعي المحوسب (CT) ، والتصوير بالرنين المغناطيسي (MRI) ، والتصوير المقطعي بالإصدار البوزيتروني (PET) ، لها بعض القيود. فهي ضخمة الحجم ومكلفة وتستخدم الإشعاع المؤين في حالة التصوير المقطعي المحوسب والتصوير المقطعي بالإصدار البوزيتروني ، مما يزيد من خطر الإصابة بالسرطان. التصوير بالموجات الدقيقة هو أسلوب جديد يبعث على الأمل يمكنه التغلب على هذه القيود. نظام الموجات الدقيقة منخفض التكلفة ، ويستخدم إشعاعات غير مؤينة. ومع ذلك ، فإنه لا زال هناك تحديات يجب التغلب عليها قبل ان يصبح هذا النظام جاهزا للاستخدام في المستشفيات. من ضمن هذه التحديات ان الصورة المعاد بناؤها ، ذات دقة منخفضة وغير واضحة بسبب استخدام التردد المنخفض وبسبب القصور في خوارزميات إعادة بناء الصور. هذا يجعل من الصعب الكشف عن الورم وتحديد موقعه ، خاصة في مراحله المبكرة. علاوة على ذلك ، فان اتخاذ القرار يعتمد على خبرة الطبيب.

هذه الرسالة تقترح استخدام التعلم العميق للتشخيص التلقائي لوجود الورم من عدمه وتحديد حجمه وموقعه مباشرة من البيانات التي تم جمعها من نظام التصوير بالموجات الدقيقة. تم تصميم نظام التصوير بالموجات الدقيقة ومحاكاته في برنامج CST باستخدام ستة هوائيات Vivaldi موزعة حول نموذج الرأس تعمل بمدى تردد يتراوح من 1.5 إلى 4.5 جيجاهرتز. تم اخذ 628 حالة ، تمثل 308 حالة منها وجود أورام بأحجام مختلفة يتراوح نصف قطرها من 0.2 مم إلى 12 مم في 28 موقعًا مختلفًا في المستوى x-z. اما الـ 320 حالة المتبقية فهي تمثل عدم وجود أورام . تم تقسيم البيانات إلى مجموعة تدريب ومجموعة اختبار. تم تدريب شبكة عصبية تلافيفية تحتوي على 12 مرشحًا ، كل منها بحجم 3×3 ، على مجموعة التدريب ثم تم اختبارها باستخدام مجموعة الاختبار. كانت النتائج واعدة ، حيث تمكنت الشبكة المصممة CNN من اكتشاف وجود الورم من عدمه بدقة 100 % في كل من مجموعات التدريب والاختبار. كانت أيضًا قادرة على تحديد نصف قطر الورم بخطأ جذر متوسط التربيع (RMSE) صغير يصل إلى 0.15 مم وتحديد الموقع في الاتجاه z باستخدام RMSE يبلغ 3.15 مم.

إقرار لجنة المناقشة

نشهد بأننا أعضاء لجنة التقويم والمناقشة قد اطلعنا على هذه الرسالة الموسومة (كشف ورم الدماغ عن طريق التصوير بالموجات الدقيقة باستخدام التعلم العميق) وناقشنا الطالب (حيدر صلاح محمود) في محتوياتها وفيما له علاقة بها بتاريخ / / 2023 وقد وجدناه جديراً بنيل شهادة الماجستير-علوم في اختصاص هندسة الاتصالات.

التوقيع:
عضو اللجنة:
التاريخ: / / 2023

التوقيع:
رئيس اللجنة:
التاريخ: / / 2023

التوقيع:
عضو اللجنة(المشرف):
التاريخ: / / 2023

التوقيع:
عضو اللجنة:
التاريخ: / / 2023

قرار مجلس الكلية

اجتمع مجلس كلية هندسة الالكترونيات بجلسته المنعقدة بتاريخ: / / 2023
وقرر المجلس منح الطالب شهادة الماجستير علوم في اختصاص هندسة الاتصالات.

مقرر المجلس: / / 2023
التاريخ: / / 2023
رئيس مجلس الكلية:
التاريخ: / / 2023

إقرار المشرف

نشهد بأن هذه الرسالة الموسومة (كشف ورم الدماغ عن طريق التصوير بالموجات الدقيقة باستخدام التعلم العميق) والمعدة من قبل الطالب (حيدر صلاح محمود) تحت اشرافنا في قسم هندسة الاتصالات / كلية هندسة الالكترونيات / جامعة نينوى، كجزء من متطلبات نيل شهادة الماجستير علوم في هندسة الاتصالات.

التوقيع: / / 2023
الاسم: أ.م.د يونس محمود عبوش
التوقيع: / / 2023
الاسم: أ.م.د ضياء محمد علي
التاريخ: / / 2023

إقرار المقوم اللغوي

اشهد بأنه قد تمت مراجعة هذه الرسالة من الناحية اللغوية وتصحيح ماورد فيها من أخطاء لغوية وتعبيرية وبذلك أصبحت الرسالة مؤهلة للمناقشة بقدر تعلق الأمر بسلامة الأسلوب أو صحة التعبير.

التوقيع:
الاسم:
التاريخ: / / 2023

إقرار رئيس قسم هندسة الاتصالات

بناءً على التوصيات المقدمة من قبل المشرف والمقوم اللغوي أشرح هذه الرسالة للمناقشة.

التوقيع:
الاسم: أ.م.د محمود احمد محمود
التاريخ: / / 2023

إقرار رئيس لجنة الدراسات العليا

بناءً على التوصيات المقدمة من قبل المشرف والمقوم اللغوي و رئيس قسم هندسة الاتصالات أشرح هذه الرسالة للمناقشة.

التوقيع:
الاسم:
التاريخ: / / 2023



جامعة نينوى
كلية هندسة لالكترونيات

كشف ورم الدماغ عن طريق التصوير بالموجات الدقيقة باستخدام التعلم العميق

رسالة تقدم بها

حيدر صلاح محمود

الى مجلس كلية هندسة الالالكترونيات

جامعة نينوى

كجزء من متطلبات نيل شهادة الماجستير في علوم

هندسة الاتصالات

بإشراف

أ.م.د. يونس محمود عبوش

أ.م.د. ضياء محمد علي

1445 هـ

2023م



جامعة نينوى
كلية هندسة الالالكترونيات

كشف ورم الدماغ عن طريق التصوير بالموجات الدقيقة باستخدام التعلم العميق

حيدر صلاح محمود

رسالة ماجستير علوم في
هندسة الاتصالات

بإشراف

أ.م.د. يونس محمود عبوش
أ.م.د. ضياء محمد علي

1445 هـ

2023م